1 **Global Soil Consumption of Atmospheric Carbon Monoxide:**

2 **An Analysis Using a Process-Based Biogeochemistry Model**

3 Licheng Liu[1], Qianlai Zhuang[1,2], Qing Zhu[1,3], Shaoqing Liu[1,4], Hella van Asperen[5], Mari

4 Pihlatie[6,7]

[1]Department of Earth, Atmospheric, Planetary Sciences, Purdue University, West Lafayette, IN 47907,

USA

[2]Department of Agronomy, Purdue University, West Lafayette, IN 47907, USA

[3] Climate Sciences Department, Climate & Ecosystem Sciences Division, Lawrence Berkeley National

Laboratory, Berkeley, CA 94720, USA

[4]Department of Earth Sciences, University of Minnesota, Minneapolis, MN, 55455, USA

[5]Institute of Environmental Physics, University of Bremen, Otto-Hahn-Allee 1, Bremen, 28359, Germany

[6]Department of Physics, University of Helsinki, P.O. Box 48, 00014 University of Helsinki, Finland

[7]Department of Forest Sciences, P.O. Box27, 00014 University of Helsinki, Finland

5 *Correspondence to:* Qianlai Zhuang(qzhuang@purdue.edu)

Abstract: Carbon monoxide (CO) plays an important role in controlling the oxidizing capacity of the atmosphere by reacting with OH radicals that affect atmospheric methane (CH_4) dynamics. We develop a process-based biogeochemistry model to quantify the CO exchange between soils and the atmosphere with a 5-minute internal time step at the global scale. The model is parameterized using the CO flux data from the field and laboratory experiments for eleven representative ecosystem types. The model is then extrapolated to global terrestrial ecosystems using monthly climate forcing data. Global soil gross consumption, gross production, and net flux of the atmospheric CO are estimated to be from -197 to -180, 34 to 36, and -163 to -145   Tg CO yr^{-1} (1Tg = 10^{12} g), respectively, when the model is driven with satellite-based atmospheric CO concentration data during 2000-2013. Tropical evergreen forest, savanna and deciduous forest areas are the largest sinks at 123 Tg CO yr^{-1}. The soil CO gross consumption is sensitive to air temperature and atmospheric CO concentration while the gross production is sensitive to soil organic carbon (SOC) stock and air temperature. By assuming that the spatially-distributed atmospheric CO concentrations (~128 ppbv) are not changing over time, the global mean CO net deposition velocity is estimated to be 0.16-0.19 mm s^{-1} during the 20th century. Under the future climate scenarios, the CO deposition velocity will increase at a rate of 0.0002-0.0013 mm s^{-1} yr^{-1} during 2014-2100, reaching 0.20-0.30 mm s^{-1} by the end of the 21st century, primarily due to the increasing temperature. Areas near the equator, Eastern US, Europe and eastern Asia will be the largest sinks due to optimum soil moisture and high temperature. The annual global soil net flux of atmospheric CO is primarily controlled by air temperature, soil temperature, SOC and atmospheric CO concentrations, while its monthly variation is mainly determined by air temperature, precipitation, soil temperature and soil moisture.

1. Introduction

Carbon monoxide (CO) plays an important role in controlling the oxidizing capacity of the atmosphere by reacting with OH radicals (Logan et al., 1981; Crutzen, 1987; Khalil & Rasmussen, 1990; Prather et al., 1995; Prather & Ehhalt, 2001). CO in the atmosphere can directly and indirectly influence the fate of critical greenhouse gases such as methane (CH_4) and ozone (O_3) (Tan and Zhuang, 2012). Although CO itself absorbs only a limited

39 amount of infrared radiation from the Earth, the cumulative indirect radiative forcing of CO

40 may be even larger than that of the third powerful greenhouse gas, nitrous oxide (N_2O,

41 Myhre et al., 2013). Current estimates of global CO emissions from both anthropogenic

42 and natural sources range from 1550 to 2900 Tg CO yr^{-1}, which are mainly from

43 anthropogenic and natural direct emissions and from the oxidation of methane and other

44 Volatile Organic Compounds (VOC) (Prather et al., 1995; Khalil et al., 1999; Bergamaschi

45 et al., 2000; Prather & Ehhalt, 2001, Stein et al., 2014). Chemical consumption of CO by

46 atmospheric OH and the biological consumption of CO by soil microbes are two major

47 sinks of the atmospheric CO (Conrad, 1988; Lu & Khalil, 1993; Yonemura et al., 2000;

48 Whalen & Reeburgh, 2001).

49   Soils are globally considered as a major sink for CO due to microbial activities

50 (Whalen and Reeburgh, 2001; King and Weber, 2007). A diverse group of soil microbes

51 including carboxydotrophs, methanotrophs and nitrifiers are capable of oxidizing CO

52 (King and Weber, 2007). Annually, 10-25% of total earth surface CO emissions were

53 consumed by soils (Sanhueza et al., 1998; King, 1999a; Chan & Steudler, 2006). Potter

54 et al. (1996) reported the global soil consumption to be from -50 to -16 Tg CO yr^{-1}

55 (negative values represent the uptake from the atmosphere to soil), by using a single-box

56 model over the upper 5 cm of soils. All existing estimates have large uncertainties and

57 range from -640 to -16 Tg CO yr^{-1} (Sanhueza et al., 1998; King, 1999; Bergamaschi et

58 al., 2000). Similarly, the estimates of CO dry deposition velocities also have large

59 uncertainties and range from 0 to 4.0 mm s^{-1}, here positive values represent deposition

60 to soils (King, 1999a; Castellanos et al., 2011). Soils also produce CO mainly via abiotic

61 processes such as thermal- and photo-degradation of organic matter or plant materials

62 (Conrad and Seiler, 1985b; Tarr et al., 1995; Schade et al., 1999; Derendorp et al., 2011;

63 Lee et al., 2012; van Asperen et al., 2015; Fraser et al., 2015, Pihlatie et al., 2016), except

64 for a few cases of anaerobic formation. Photo-degradation is identified as radiation-

65 dependent degradation due to absorbing radiation (King et al., 2012). Thermal-

66 degradation is identified as the temperature-dependent degradation of carbon in the

67 absence of radiation and possibly oxygen (Derendorp et al., 2011; Lee et al., 2012; van

68 Asperen et al., 2015; Pihlatie et al., 2016). These major soil CO production processes,

together with soil CO consumption processes, have not been adequately considered in global soil CO budget estimates.

To date, most top-down atmospheric models applied a dry deposition scheme based on the resistance model of Wesely (1989). Such schemes provided a wide range of dry deposition velocities (Stevenson et al., 2006). Only a few models (MOZART-4, Emmons et al., 2010; CAM-chem, Lamarque et al., 2012) have extended their dry deposition schemes with a parameterization for CO and H_2 uptake through oxidation by soil microbes, following the work of Sanderson et al. (2003), which was based on extensive measurements from Yonemura et al. (2000). Potter et al. (1996) developed a bottom-up model to simulate CO consumption and production at the global scale. Their model is a single box model, only considers top 5 cm depth of soil and does not have explicit microbial factors, therefore might have underestimated CO consumption (Potter et al., 1996; King, 1999a). Current bottom-up CO modeling approaches are mostly based on a limited number of CO *in situ* observations or laboratory studies to quantify regional and global soil consumption (Potter et al., 1996; Sanhueza et al., 1998; Khalil et al., 1999; King, 1999a; Bergamaschi et al., 2000; Prather & Ehhalt, 2001). To our knowledge, no detailed process-based model of soil-atmospheric exchange of CO has been published in the recent 15 years. One reason is that there is an incomplete understanding of biological processes of uptake (King & Weber, 2007; Vreman et al., 2011; He and He, 2014; Pihlatie et al., 2016). Another reason is that there is a lack of long-term CO flux measurements for different ecosystem types to calibrate and evaluate the models. CO flux measurements are mostly from short-term field observations or laboratory experiments (e.g. Conrad and Seiler, 1985a; Funk et al., 1994; Tarr et al., 1995; Zepp et al., 1997; Kuhlbusch et al., 1998; Moxley and Smith, 1998; Schade et al., 1999; King and Crosby, 2002; Varella et al., 2004; Lee et al., 2012; Bruhn et al., 2013; van Asperen et al., 2015). The first study to report long-term and continuous field measurements of CO flux over grasslands using a micrometeorological eddy covariance (EC) method is Pihlatie et al. (2016).

To improve the quantification of the global soil CO budget for the period 2000-2013 and the CO deposition velocity for the 20th and 21st centuries, this study developed a CO dynamics module (CODM) embedded in a process-based biogeochemistry model,

100 the Terrestrial Ecosystem Model (TEM) (Zhuang et al., 2003, 2004, 2007). CODM was

101 then calibrated and evaluated using laboratory experiments and field measurements for

102 different ecosystem types. The atmospheric CO concentration data from MOPITT (Gille,

103 2013) were used to drive model simulations from 2000 to 2013. A set of century-long

104 simulations of 1901-2100 were also conducted using the atmospheric CO concentrations

105 estimated with an empirical function (Badr & Probert, 1994; Potter et al., 1996). Finally,

106 the effects of multiple forcings on the global CO consumption and production, including

107 the changes of climate and atmospheric CO concentrations at the global scale were

108 evaluated with the model.

109

110 **2. Method**

111 **2.1 Overview**

112 We first developed a soil CO dynamics module (CODM) on a daily time step that

113 considers: (1) the soil-atmosphere CO exchange and diffusion process between soil

114 layers, (2) the consumption by soil microbial oxidation, (3) the production by soil chemical

115 oxidation, and (4) the effects of temperature, soil moisture, soil CO substrate and surface

116 atmospheric CO concentration on these processes. Second, we used the observed soil

117 temperature and moisture to evaluate TEM hydrology module and the soil thermal module

118 in order to estimate soil physical variables. Then we used the data from laboratory

119 experiments and CO flux measurements to parameterize the model using the Shuffled

120 Complex Evolution (SCE-UA) method (Duan et al., 1993). Finally, the model was

121 extrapolated to the globe at a 0.5° by 0.5° resolution. We conducted three sets of model

122 experiments to investigate the impact of climate and atmospheric CO concentrations on

123 soil CO dynamics: 1) Simulations for 2000-2013 with MOPITT satellite atmospheric CO

124 concentration data; 2) Simulations for 1901-2100 with constant atmospheric CO

125 concentrations estimated from an empirical function and the historical climate data (1901-

126 2013) and three future climate scenarios (2014-2100); and 3) Eight sensitivity simulations

127 by increasing and decreasing a) constant CO surface concentrations by 30%, b) SOC by

128 5%, c) precipitation by 20% and d) air temperature by 3°C for each pixel, respectively,

129 while holding other forcing data as they were, during 1999-2000.

2.2 Carbon Monoxide Dynamics Module (CODM)

131

132   Embedded in TEM (Figure 1), CODM is mainly driven by: (1) soil organic carbon
133   availability based on a carbon and nitrogen dynamics module (CNDM) (Zhuang et al.,
134   2003); (2) soil temperature profile from a soil thermal module (STM) (Zhuang et al., 2001,
135   2003); and (3) soil moisture profile from a hydrological module (HM) (Bonan, 1996;
136   Zhuang et al, 2004). The net exchange of CO between the atmosphere and soil is
137   determined by the mass balance approach (net flux = total production – total oxidation –
138   total soil CO concentration change). According to previous studies, we separated active
139   soils (top 30 cm) for CO consumption and production into 1 cm thickness layers (King,
140   1999a, 1999b; Whalen & Reeburgh, 2001; Chan & Steudler, 2006). Between the soil
141   layers, the changes of CO concentrations were calculated as:

142
$$\frac{\partial(C(t,i))}{\partial t} = \frac{\partial}{\partial z}\left(D(t,i)\frac{\partial\big(C(t,i)\big)}{\partial z}\right) + P(t,i) - O(t,i) \qquad (1)$$

143   Where $C(t,i)$ is the CO concentration (mg m^{-3}) in layer i and at time t. z is the depth of
144   the soil (m). $D(t,i)$ is the diffusion coefficient (m^2 s^{-1}) for layer i. $P(t,i)$ is the CO
145   production rate (mg m^{-3} s^{-1}) and $O(t,i)$ is the CO consumption rate (mg m^{-3} s^{-1}). $D(t,i)$ is
146   calculated using the method from Potter et al. (1996), which is a function of soil
147   temperature, soil texture and soil moisture. The upper boundary condition is the
148   atmospheric CO concentration, which is estimated with an empirical function of latitude
149   (Potter et al., 1996) or directly measured by the MOPITT satellite during 2000-2013. The
150   lower boundary condition is assumed to have no diffusion exchange with the layer
151   underneath. This partial differential equation (PDE) is solved using the Crank-Nicolson
152   method for less time-step-sensitive solution.

153   The CO consumption was modeled in unsaturated soil pores as:

154
$$O(t,i) = V_{max} \cdot f_1\big(C(t,i)\big) \cdot f_2\big(T(t,i)\big) \cdot f_3\big(M(t,i)\big) \qquad (2)$$

155   Where V_{max} is the ecosystem specific maximum oxidation rate and was estimated
156   previously ranging from 0.3 to 11.1 μg CO g^{-1} h^{-1} for different ecosystems (Whalen &
157   Reeburgh, 2001). f_i represents the effects of soil CO concentration $C(t,i)$, temperature
158    $T(t,i)$ and moisture $M(t,i)$ on the CO soil consumption. Considering the CO consumption

159   as the result of microbial activities, we calculated $f_1(C(t,i))$, $f_2(T(t,i))$ and $f_3(M(t,i))$

160   in a similar way to Zhuang et al. (2004):

161    $$f_1(C(t,i)) = \frac{C(t,i)}{C(t,i) + k_{CO}} \qquad (2.1)$$

162    $$f_2(T(t,i)) = Q_{10}^{\frac{T(t,i)-T_{ref}}{10}} \qquad (2.2)$$

163    $$f_3(M(t,i)) = \frac{(M(t,i) - M_{min})(M(t,i) - M_{max})}{(M(t,i) - M_{min})(M(t,i) - M_{max}) - (M(t,i) - M_{opt})^2} \qquad (2.3)$$

164   Where $f_1(C(t,i))$ is a multiplier that enhances the oxidation rate with increasing soil CO

165   concentrations using a Michaelis-Menten function with a half-saturation constant k_{CO}, and

166   their values were previously estimated ranging from 5 to 51 µl CO l^{-1} for different

167   ecosystems (Whalen & Reeburgh, 2001); $f_2(T(t,i))$ is a multiplier that enhances the CO

168   oxidation rate with increasing soil temperature using a Q10 function with Q_{10} coefficients

169   (Whalen & Reeburgh, 2001). T_{ref} is the reference temperature, units are °C (Zhuang et

170   al., 2004, 2013). $f_3(M(t,i))$ is a multiplier to estimate the biological limiting effect that

171   diminishes the CO oxidation rates if the soil moisture is not at an optimum level (M_{opt}).

172   M_{min}, M_{max} and M_{opt} are the minimum, maximum and optimum volumetric soil moistures

173   of oxidation reaction, respectively. Equation (2.2) will overestimate the CO consumption

174   at high temperature because in reality the CO consumption will decrease when

175   temperature is higher than optimum temperature, while f_2 will keep increasing with rising

176   temperature. However, the CO consumption is constrained by the CO production, and

177   equation (1) is used to represent this constraint.

178   We modeled the CO production rate ($P(t,i)$) as a process of chemical oxidation

179   constrained by the soil organic carbon (SOC) decay (Conrad and Seiler,1985; Potter et

180   al. 1996; Jobbagy & Jackson, 2000; van Asperen et al., 2015):

181    $$P(t,i) = P_r(t,i) \cdot E_{SOC} \cdot C_{SOC}(t) \cdot F_{SOC} \qquad (3)$$

182   Where $P_r(t,i)$ is a reference soil CO production rate which has been normalized to the

183   rate at reference temperature (the production rate at temperature (t,i) divided by the

184   production rate at the reference temperature), which is affected by soil moisture and soil

185   temperature (Conrad and Seiler,1985; van Asperen et al., 2015). E_{SOC} is an estimated

186 nominal CO production factor of 3.5 ± 0.9 X 10^{-9} mg CO m^{-2} s^{-1} per g SOC m^{-2} (to 30 cm

187 soil depth) (Potter et al., 1996). $C_{SOC}(t)$ is a SOC content (mg m^{-2}), which is provided by

188 CNDM module in TEM. F_{SOC} is a constant fraction of top 30cm SOC compared to the total

189 amount of SOC, which is 0.33 for shrubland areas, 0.42 for grassland areas and 0.50 for

190 forest areas, respectively (Jobbagy & Jackson, 2000). $P_r(t, i)$ was calculated as:

191
$$P_r(t, i) = \exp\left(f_4\big(M(t, i)\big) \cdot Ea_{ref}/R \cdot \left(\frac{1}{273.15 + PT_{ref}} - \frac{1}{T(t, i) + 273.15} \right) \right) \quad (3.1)$$

192
$$f_4\big(M(t, i)\big) = \frac{PM_{ref}}{M(t, i) + PM_{ref}} \quad (3.2)$$

193 Where equation (3.1) is derived from the Arrhenius equation for chemical reactions and

194 normalized using the reference temperature PT_{ref}. Ea_{ref}/R is the reference activation

195 energy divided by gas constant R, units are K. $f_4\big(M(t, i)\big)$ is the multiplier that reduces

196 activation energy using a regression approach based on the laboratory experiment of

197 moisture influences on CO production (Conrad and Seiler,1985). PM_{ref} is the reference

198 volumetric soil moisture, ranging from 0.01 to 0.5 volume/volume (v/v). We assumed the

199 thermal-degradation as the main CO producing process due to lack of photo-degradation

200 data and hard to distinguish photo-degradation from observations. In order to reduce the

201 bias from the thermal-degradation to the total abiotic degradation, the equation (3.1) is

202 parameterized by comparing with the total production rate. For instance, $P_r(t, i)$

203 calculation can perfectly fit the experiment results in Van Asperen et al. (2015) with proper

204 PT_{ref}(18°C), Ea_{ref}/R(14000 K), and PM_{ref}(0.5 v/v).

205   The CO deposition velocity was modeled in the same way as equation (19.1) in

206 Seinfeld et al. (1998):

207
$$v_d = -F_{net}/C_{CO,air} \quad (4)$$

208 Where v_d is the CO deposition velocity (mm s^{-1}). F_{net} is the model estimated CO net flux

209 rate (mg CO m^{-2} day^{-1}). $C_{CO,air}$ is the CO surface concentration (ppbv). $C_{CO,air}$ can be

210 MOPITT CO surface concentration data or the derived CO surface concentrations using

211 the same method as Potter et al. (1996). Positive values of v_d represent soil uptake

212 (deposition from air to soils) and negative values represent soil emissions.

213

2.3 Model Parameterization and Extrapolation

The model parameterization was conducted in two steps: 1) Thermal and hydrology modules embedded in TEM were revised, calibrated and evaluated by running model driven by corresponding local meteorological or climatic data at four representative sites, including boreal forest, temperate forest, tropical forest and savanna (Table 1, site No.1 to 4, Figure 2) to minimize model-data mismatch in terms of soil temperature and moisture. 2) CODM module was parameterized by running TEM for observational periods driven with the corresponding local meteorological or climatic data at each reference site (Table 1, Figure 3), and using the Shuffled Complex Evolution Approach in R language (SCE-UA-R) (Duan et al., 1993) to minimize the difference between the simulated and observed net CO flux. Eleven parameters including k_{CO}, V_{max}, T_{ref}, Q_{10}, M_{min}, M_{max}, M_{opt}, E_{SOC}, Ea_{ref}/R, PM_{ref} and PT_{ref} were optimized (Table 2). To be noticed, F_{SOC} was not involved in the calibration process. Parameter priors were decided based on previous studies (Conrad & Seiler, 1985; King, 1999b; Whalen & Reeburgh, 2001; Zhuang et al., 2004). The SCE-UA-R was used for site No. 6, 8, 10, 11 (Table 1). In parameter ensemble simulations, we have run 50 times SCE-UA-R with 10000 maximum loops for each site, and all of them have reached stable state before the end of the loops. For wetlands, the only available data for calibration is from site No.12. We used the trial-and-error method to make the simulated results in the range of observed flux rates, with a 10% tolerance. For tropical sites, since tropical savanna vegetation type is treated as a combination type of tropical forest and grassland in our simulations, we first used Site No. 13 to set priors to fit the experiment results with a 10% tolerance and then evaluated by running our model comparing with site No.7 results. Site No. 9 and 5 were used to evaluate our model results for temperate forest and grassland. Besides the observed climatic and soil property data, we used the ERA-Interim reanalysis data from The European Centre for Medium-Range Weather Forecasts (ECMWF) (Dee et al., 2011), AmeriFlux observed meteorology data (http://ameriflux.lbl.gov/) and reanalysis climatic data from Climatic Research Unit (CRU, Harris et al., 2013) to fill the missing environmental data. To sum up, parameters for various ecosystem types in Table 2 were the final results of our parameterization. Model parameterization was conducted for ecosystem types including boreal forest, temperate coniferous forest, temperate

245 deciduous forest, and grassland using SCE-UA-R. In contrast, for tropical forest and wet

246 tundra, we used a trial-and-error method to adjust parameters to allow model simulation

247 best fit the observed data. Due to limited data availability, we assumed temperate

248 evergreen broadleaf forests have the same parameters as temperate deciduous forest

249 ecosystems.

250

251 **2.4 Data Organization**

252 To get the spatially and temporally explicit estimates of the CO consumption,

253 production and net flux at the global scale, we used the data of land cover, soils, climate

254 and leaf area index (LAI) from various sources at a spatial resolution of 0.5° latitude X

255 0.5° longitude to drive TEM. The land cover data include the potential vegetation

256 distribution (Melillo et al., 1993) and soil texture (Zhuang et al., 2003), which were used

257 to assign vegetation- and texture-specific parameters to each grid cell.

258 For the simulation of the period 1901-2013, the monthly air temperature,

259 precipitation, clouds fraction and vapor pressure data sets from CRU were used to

260 estimate the soil temperature, soil moisture and SOC with TEM (Figure 4). The monthly

261 LAI data from TEM were required to simulate soil moisture (Zhuang et al., 2004). During

262 this period time, we used an empirical function of latitude, which was derived from the

263 observed latitudinal distribution of tropospheric carbon monoxide (Badr and Probert, 1994)

264 to calculate static CO surface concentration distribution (equation (7), Potter et al., 1996):

265 $$C_{CO,air} = 82.267856 + 0.8441503L + 1.55934 \times 10^{-2}L^2 + 2.37 \times 10^{-5}L^3 -$$

266 $$2.3 \times 10^{-6}L^4 \qquad (5)$$

267 Where $C_{CO,air}$ is the derived surface CO concentration (ppbv), *L* represents

268 latitudes with negative degrees for southern hemisphere and positive degrees for

269 northern hemisphere. We also used the atmospheric CO data from MOPITT satellite

270 during 2000-2013 (Figure 5). We averaged day-time and night-time monthly mean values

271 of CO surface level 3 retrieval data (variables mapped on 0.5° latitude X 0.5° longitude

272 grid scales with monthly time step, Gille, 2013) to represent the CO surface concentration

273 level in each month. The pixels with missing values were filled with the average values

274 of those pixels that were inside 1.5 times of the distance between the missing-value pixel

275 and the nearest pixel with values. These global mean values shown in Figure 5 do not

276 include ocean surfaces, thus there are differences between our surface CO concentration

277 results and Yoon and Pozzer's report in 2014, which is as low as 99.8 ppb. From 2014 to

278 2100, we used the Intergovernmental Panel on Climate Change (IPCC) future climate

279 scenarios from Representative Concentration Pathways (RCPs) climate forcing data sets

280 RCP2.6, RCP4.5 and RCP8.5 (Figure 6). RCP2.6, 4.5 and 8.5 datasets are future climate

281 projections with anthropogenic greenhouse gas emission radiative forcing of 2.6 W m^{-2},

282 4.5 W m^{-2} and 8.5 W m^{-2}, respectively, by 2100. Since RCPs did not have water vapor

283 pressure data, we used the specific humidity and sea level air pressure from the RCPs

284 and elevation of surface to estimate the monthly surface vapor pressure (Seinfeld &

285 Pandis, 1998).

286

287 **2.5 Model Experiment Design**

288 We conducted two sets of core simulations and eight sensitivity test simulations

289 for a historical period. The two core sets of simulations were driven with the MOPITT CO

290 surface concentrations data for the period 2000-2013 (experiment E1) and with the

291 spatially distributed CO surface concentrations assuming as constant over time estimated

292 from an empirical function of latitude for the period 1901-2100 (experiment E2),

293 respectively. Specifically, in experiment E2 we used the CRU climate forcing for the

294 historical period 1901-2013 and the climate data of RCP2.6, RCP4.5 and RCP8.5 for

295 different future scenarios to examine the responses of CO flux to changing climates. Eight

296 sensitivity simulations were driven with varying different forcing variables while keeping

297 others as they were: 1) with constant CO surface concentrations ± 30%, 2) SOC ± 5%, 3)

298 precipitation ± 20% and 4) air temperature ± 3°C for each pixel, respectively, during 1999-

299 2000 (E3).

300

301 **3. Results**

302 **3.1 Site Evaluation**

303 Both the magnitude and variation of the simulated soil temperature and moisture

304 from cold areas to warm areas are compared well to the observations (Figure 2). The

305 magnitude of the simulated CO flux is comparable and correlated with the observations

306 (R is about 0.5, p-value < 0.001, Figures 3, a2, b2, c2, d2). Estimated CO fluxes for

307 different ecosystem types range from -28.4 to 1.7 mg CO m^{-2} day^{-1}, and the root mean

308 square error (RMSE) between simulation and observation at all sites is below 1.5 mg CO

309 m^{-2} day^{-1}. RMSE for site No. 7 is bigger than 2.0 mg CO m^{-2} day^{-1} when compared with

310 transparent chamber observations. For boreal forest site, we only had 8 acceptable

311 points in 1994 and 1996 (Figure 3c2).

312

313 **3.2 Global Soil CO Dynamics During 2000-2013**

314   Using the MOPITT CO surface concentration data during 2000-2013 (E1), the

315 estimated mean soil CO consumption, production and net flux (positive values indicate

316 CO emissions from soils to the atmosphere) are from -197 to -180, 34 to 36 and -163 to

317 -145 Tg CO yr^{-1}, respectively (Figure 7a). The consumption is about 4 times larger than

318 the production. The annual consumption and net flux trends follow the atmospheric CO

319 concentration trends (Figure 5b, Figure 7a), with a small interannual variability (< 10%).

320 The latitudinal distributions of the consumption, production and net fluxes share the same

321 spatial pattern. Around 20°S-20°N and 20-60°N are the largest and second largest areas

322 for production and consumption, while the 45°S-45°N area accounts for nearly 90% of

323 the total consumption and production (Figure 7b, Table 3). The Southern and Northern

324 Hemispheres have 41% and 59% of the total consumption, and 47% and 53% of the total

325 production, respectively (Table 3). The highest rates of the consumption and production

326 are located in areas close to the equator, and the consumption from areas such as

327 eastern US, Europe and eastern Asia also is high (< -1000 mg m^{-2} yr^{-1}) (Figure 8a, b).

328 Global soils serve as an atmospheric CO sink (Figure 8c). Some areas, such as western

329 US and southern Australia, are CO sources, all of which are grasslands or experiencing

330 dry climate. Tropical evergreen forests are the largest sinks, consuming 86 Tg CO yr^{-1},

331 and tropical savanna and deciduous forest are the second and third largest sinks,

332 consuming a total of 37 Tg CO yr^{-1} (Table 4). These three ecosystems account for 66%

333 of the total consumption. Tropical evergreen forests are also the largest source of soil CO

334 production, producing 16 Tg CO yr^{-1}, while tropical savanna has a considerable

335 production of 6 Tg CO yr^{-1} (Table 4). Moreover, tropical areas, including forested wetlands,

forested floodplain and evergreen forests, are most efficient for the CO consumption, ranging from -18 to -13 mg CO m^{-2} day$^{-1.}$ They are also most efficient for the CO production at over 2 mg CO m^{-2} day^{-1} (Table 4, calculated by fluxes divided by area).

3.3 Global Soil CO Dynamics During 1901-2100

Using the constant CO surface concentration, the estimated global mean CO deposition velocities are 0.16-0.19 mm s^{-1} for the period 1901-2013. For the period 2014-2100, the deposition velocities are 0.18-0.21, 0.18-0.24 and 0.17-0.31 for RCP2.6, 4.5 and 8.5 scenarios, respectively (Figure 9). During 2014-2100, there are significant trends of increasing deposition velocities for nearly all scenarios (Figure 9). The rates of increasing are 0.0002, 0.0005 and 0.0013 mm s^{-1} yr^{-1}, and will reach 0.20, 0.23 and 0.30 mm s^{-1} by the end of the 21st century for the RCP2.6, RCP4.5 and RCP8.5 scenarios, respectively (Figure 9). These increasing trends are similar to the air temperature increasing trends (Figure 6a). The global distribution patterns of the CO deposition velocity are similar to the net flux distribution for the period 2000-2013 but there are significant differences among the 1901-2013, RCP2.6, RCP4.5 and RCP8.5 scenarios (Figure 10). The deposition velocities are increasing from the RCP2.6 to RCP8.5 and larger than that in the historical periods in areas near the equator (Figure 10). Areas near the equator and eastern Asia become big sinks of the atmospheric CO, while northeastern US becomes a small source in the 21st century (Figure 10). Different vegetation types have a large range of the deposition velocity, from 0.008 to 1.154 mm s^{-1} (Table 4). The tropical forested wetland, tropical forested floodplain and tropical evergreen forest have top three largest deposition velocity of 1.154, 1.117 and 0.879 mm s^{-1}, respectively, while desert, short grasslands, and wet tundra have the smallest deposition velocity of 0.008, 0.010 and 0.015 mm s^{-1}, respectively.

3.4 Sensitivity test

The soil CO consumption is most sensitive (changing 29%) to air temperature while the production is most sensitive to both air temperature (changing up to 36%) and SOC (5%). The net CO fluxes have the similar sensitivities as the consumption. The

366 annual CO consumption, production and net flux follow the change of air temperature

367 (Table 5). In addition, a 30% change in precipitation will not lead to large changes in the

368 CO flux (< 3%).

369

370 **4. Discussion**

371 **4.1 Comparison with Other Studies**

372 Previous studies estimated a wide range of the global CO consumption from -16

373 to -640 Tg CO yr^{-1}. Our estimates are from -197 to -180 Tg CO yr^{-1} for 2000-2013 using

374 the MOPITT satellite CO surface concentration data. Previous studies also provided a

375 large range for the CO production from 0 to 7.6 mg m^{-2} day^{-1} (reviewed in Pihlatie et al.,

376 2016). Our results showed the averaged CO production ranging from 0.01 to 2.29 mg m^{-2}

377 ^{2} day^{-1}. The existing estimates of the CO deposition velocities for different vegetation

378 types ranged from 0.0 to 4.0 mm s^{-1} while our simulations showed an averaged CO

379 deposition velocity ranging from 0.006 to 1.154 mm s^{-1} for different vegetation types. The

380 large uncertainty of these estimates is mainly due to different considerations of the

381 microbial activities, the depth of the soil, and the parameters in the model. In contrast to

382 the estimates of -57 to -16 Tg CO yr^{-1} which were based on top 5 cm soils (Potter et al.,

383 1996), our estimates considered 30 cm soils, which were used in Whalen & Reeburgh

384 (2001). In addition, we used a thinner layer division (1 cm each layer) for diffusion process,

385 and used the Crank-Nicolson method to solve partial differential equations to avoid time

386 step influences. We also included the microbial CO oxidation process to remove the CO

387 from the soil and considered the effects of soil moisture, soil temperature, vegetation type

388 and soil CO substrate on microbial activities. Our soil thermal, soil hydrology and carbon

389 and nitrogen dynamics simulated in TEM provided carbon substrate spatially and

390 temporally for estimating the soil CO dynamics. Overall, although a few previous studies

391 have examined the long-term impacts of climate, land use and nitrogen deposition on the

392 CO dynamics (Chan & Steudler, 2006, Pihlatie et al., 2016), the global prediction of the

393 soil CO dynamics still has a large uncertainty.

394

4.2 Major Controls to Soil CO Dynamics

The sensitivity tests indicate that the consumption is normally much larger than the CO production so that the former will determine the dynamics of the net flux (Table 5). Model being sensitive to air temperature explains the small increasing trends after the 1960s, the significant increasing trend in the 21st century and the large sinks over tropical areas (Table 5, Figure 9). SOC did not directly influence the CO consumption. For instance, increasing SOC led to an increase in soil CO substrate, implying that more CO in soils can be consumed. To be noticed, an extra 3 Tg CO yr^{-1} was taken up from the atmosphere to the soil in the sensitivity test when SOC increasing by 5% (Table 5), which will be discussed in detail in Section 4.3. CO surface concentrations will only influence the uptake rate and soil CO substrate concentrations, thus influencing the soil CO consumption rate.

The annual CO consumption and net flux have a similar correlation coefficient with forcing variables and both are significantly correlated with air temperature, soil temperature SOC and atmospheric CO concentration (R > 0.91 globally, Table 6). Increasing temperature will increase microbial activities, while more SOC will increase soil CO substrate level. The annual CO consumption and net flux have low correlations with annual precipitation and soil moisture, especially at 45°N-45°S (R < 0.54 Table 6). The annual CO production is strongly correlated with annual mean SOC, air temperature and soil temperature (R > 0.91), while is less correlated with precipitation, soil moisture and atmospheric CO concentration. Meanwhile, the monthly CO consumption, production and net flux are well correlated with air temperature, soil temperature, precipitation, and soil moisture (R > 0.69 globally Table 6). The soil moisture is significantly influenced by temperature at a monthly time step since the increasing temperature would induce higher evapotranspiration. The monthly CO consumption, production and net flux have low correlations with SOC because it will not change greatly within a month.

The R between the annual soil CO consumption and atmospheric CO concentration is 0.91 at the global scale because the atmospheric CO concentration, air temperature, and soil temperature dominate the annual consumption rate. At monthly scale, this R is -0.48 because the global atmospheric CO concentrations are high in winter and low in summer while the simulated soil CO consumption shows an opposite monthly

variation (Table 6, Figure 11), suggesting that other factors such as precipitation, air temperature, and soil temperature are major controls for the monthly CO fluxes.

4.3. Model Uncertainties and Limitations

There are a number of limitations, contributing to our simulation uncertainties. First, due to lacking long-period observational data of the CO flux and associated environmental factors, the model parameterization can only be conducted for 4 ecosystem types including boreal forest, temperate coniferous forest, temperate deciduous forest and grassland. Tropical forest calibration is only conducted using a very limited amount of laboratory experiment data, but tropical areas are hotspots for CO soil-atmosphere exchanges. Besides, the amount of tropical forest SOC for top 30 cm can be very large according to observations. TEM model may underestimate the top 30 cm SOC, which will underestimate the production rates, especially in tropical regions. Tropical regions typically have high temperature during the whole year, which may result in overestimation of the CO consumption using equation (2.2). The large deviation of model simulations to observations in tropical savanna (which is mosaic of tropical forest and grassland ecosystems) may be due to using outside air temperature to represent inside air temperature of transparent chamber observations (Varella et al., 2004), and uncertain tropical forest parameterization. Second, we used the conclusion from van Asperen et al. (2015) and only considered the thermal-degradation process for the CO production in this study. The photo-degradation process and biological formation process were not considered due to lacking the understanding of these processes. Third, the static CO surface concentration derived from the empirical function is lower than the MOPITT CO surface concentration, which will lead to underestimation of CO deposition velocity during 1901-2100. Fourth, from the sensitivity test (Table 5) we notice that an increase in SOC by 5% resulted in a net flux increase from the atmosphere to the soil by 2.57%. The SOC increase enhanced CO production (Equation 3), CO concentrations (Equation 1), and CO oxidation (Equation 2). When the change of total oxidation is larger than the difference between the change of total production and the change of total soil CO concentration (Equation 1), the estimate of the net flux change is negative (from the atmosphere to soil) using a mass balance approach (Section 2.2), which leads to a 2.57% increase in the net

flux in our SOC sensitive test. This is due to the fact that CO production (Equation 3) is calculated independently from oxidation (Equation 2). This will not influence our general findings since SOC varies only slightly during our simulation periods with a 3% increase from 1900 to 2013 (Figure 4d) and up to a 4% increase from 2014 to 2100 (Figure 6g). This model artifact that is apparent in the SOC sensitivity test can be alleviated using a very fine time step (e.g., 1 second), because in this case CO concentrations change only slightly within the short time. Therefore, when a short time step is used, the net flux roughly equals the difference between production and oxidation. If the change of production is bigger than the change of oxidation, the change of net flux will be positive, leading to a decrease of deposition to the soil. The downside is that running the model at a time step of one second will require a significantly large amount of computing time. Fifth, our model structure still has a large potential to improve. In this study we divided the top 30 cm soil into 30 layers (layer thickness dz = 1 cm), but a finer division will increase the accuracy (Figure 12). We chose 1 cm thickness because if thicker than 1 cm, the model vertical CO concentration profile will deviate from reality and diffusion process will be influenced significantly. If thinner than 1 cm, it will need much more computing time but doesn't have much improvement compared to thickness set to 1 cm (Figure 12a-e). We notice that the 30-layer division well represents the soil CO concentration profile not only in the days of soil CO net uptake, but also in the days of CO net emission (Figure 12c, f). Sixth, Michaelis-Menten function (equation 2.1) is used in this model and we notice that k_{CO} is normally much larger than $C(t, i)$ in those days of net soil uptake (over ten times larger, Figure 12). However, we can't simplify equation (2.2) to $f_1\big(C(t, i)\big) = \frac{C(t,i)}{k_{CO}}$, because the CO concentrations in the soil can be larger than in the atmosphere in the days of net emissions and $C(t, i)$ may be close to k_{CO}, and then the simplified equation may lead to overestimation of CO oxidation (Figure 12f). Finally, although we focused on natural ecosystems in this study, the land-use change, agriculture activity, and nitrogen deposition also affect the soil CO consumption and production (King, 2002; Chan & Steudler, 2006). For instance, the soil CO consumption in agriculture ecosystems is from 0 to 9 mg CO m^{-2} day^{-1} in Brazil (King & Hungria, 2002). In this study, we used grassland or forest ecosystem to represent agriculture areas in CODM module. Our future study shall include these processes and factors.

5. Conclusions

We analyzed the magnitude, spatial pattern, and the controlling factors of the atmosphere-soil CO exchanges at the global scale for the 20th and 21st centuries using a process-based biogeochemistry model. Major processes include the atmospheric CO diffusion from the atmosphere to the soil and inside the soil of terrestrial ecosystems, microbial oxidation removal of CO, and CO production through chemical reaction. We found that air temperature and soil temperature play a dominant role in determining the annual soil CO consumption and production while precipitation, air temperature, and soil temperature are the major controls for the monthly consumption and production. The atmospheric CO concentrations are important for annual CO consumption. We estimated that the global annual CO consumption, production and net fluxes for 2000-2013 are from -197 to -180, 34 to 36 and -163 to -145 Tg CO yr^{-1}, respectively, when using the MOPITT CO surface concentration data. Tropical evergreen forest, savanna and deciduous forest areas are the largest sinks accounting for 66% of the total CO consumption, while the Northern Hemisphere consumes 59% of the global total. During the 20th century, the estimated CO deposition velocity is 0.16-0.19 mm s^{-1}. The predicted CO deposition velocity will reach 0.20-0.30 mm s^{-1} in the 2090s, primarily because of the increasing air temperature. The areas near the equator, eastern Asia, Europe and eastern US will become the hotspots of sink because they have warm and moist soils. This study calls for long-period observations of CO flux for various ecosystem types and better projection of atmospheric CO surface concentrations from 1901-2100 to improve future estimates of global soil CO consumption. The effects of land-use change, agriculture activities, nitrogen deposition, photo-degradation and biological formation shall also be considered to improve future quantification of soil CO fluxes.

Acknowledgment

This study is supported through projects funded to Q.Z. by Department of Energy (DE-SC0008092 and DE-SC0007007) and the NSF Division of Information and Intelligent

518   Systems (NSF-1028291). The supercomputing resource is provided by Rosen Center for

519   Advanced Computing at Purdue University. We acknowledge Dr. Stephen C. Whalen

520   made the observational CO flux data available to this study. We are also grateful to

521   University of Tuscia (dep. DIBAF), Italy, and their affiliated members, for their help and

522   the use of their field data.

References:

Badr, O., & Probert, S. D.:Carbon monoxide concentration in the Earth's atmosphere. Applied Energy, doi:10.1016/0306-2619(94)90035-3,1994

Badr, O., & Probert, S. D.: Sinks and environmental impacts for atmospheric carbon monoxide, Applied Energy. doi:10.1016/0306-2619(95)98803-A,1995

Bartholemew, G.W., Alexander, M.: Soils as a sink for atmospheric carbon monoxide, Science 212, 1389-1391, doi:10.1126/science.212.4501.1389, 1981

Bartholomew, G. W., & Alexander, M.: Notes. Microorganisms responsible for the oxidation of carbon monoxide in soil. Environmental Science & Technology. American Chemical Society (ACS), doi:10.1021/es00099a013, 1982

Bender, M., & Conrad, R.: Microbial oxidation of methane, ammonium and carbon monoxide, and turnover of nitrous oxide and nitric oxide in soils, Biogeochemistry, Springer Nature, doi:10.1007/bf00002813, 1994

Bergamaschi, P., Hein, R., Heimann, M., & Crutzen, P. J.: Inverse modeling of the global CO cycle: 1. Inversion of CO mixing ratios, Journal of Geophysical Research: Atmospheres, doi:10.1029/1999jd900818, 2000

Bonan, G.: A Land Surface Model (LSM Version 1.0) for Ecological, Hydrological, and Atmospheric Studies: Technical Description and User's Guide, UCAR/NCAR, doi:10.5065/d6df6p5x, 1996

Bourgeau-Chavez, L.L., Garwood, G.C., Riordan, K., Koziol, B.W., Slawski, J.,: Development of calibration algorithms for selected water content reflectometry probes for burned and nonburned organic soils of Alaska. Int. J. Wildland Fire 19, 961e975, doi:10.1071/wf07175, 2012

Bruhn, D., Albert, K. R., Mikkelsen, T. N., & Ambus, P.: UV-induced carbon monoxide emission from living vegetation. Biogeosciences, Copernicus GmbH, doi:10.5194/bg-10-7877-2013, 2013

Castellanos, P., Marufu, L. T., Doddridge, B. G., Taubman, B. F., Schwab, J. J., Hains, J. C., … Dickerson, R. R.: Ozone, oxides of nitrogen, and carbon monoxide during pollution events over the eastern United States: An evaluation of emissions and vertical mixing, Journal of Geophysical Research Atmospheres, 116(16), doi:10.1029/2010JD014540, 2011

Chan, A. S. K., & Steudler, P. A.: Carbon monoxide uptake kinetics in unamended and long-term nitrogen-amended temperate forest soils. FEMS Microbiology Ecology, 57(3), 343–354, doi:10.1111/j.1574-6941.2006.00127.x, 2006

Conrad, R., & Seiler, W.: Role of Microorganisms in the Consumption and Production of Atmospheric Carbon Monoxide by Soil. Appl. Environ, Microbiol., 40(3), 437–445. Retrieved from http://aem.asm.org/cgi/content/abstract/40/3/437, 1980

Conrad, R., & Seiler, W.: Arid soils as a source of atmospheric carbon monoxide, Geophysical Research Letters, doi:10.1029/gl009i012p01353, 1982

557   Conrad, R., & Seiler, W.: Characteristics of abiological carbon monoxide formation from soil organic matter,

558   humic acids, and phenolic compounds, Environmental Science & Technology, American Chemical Society

559   (ACS), doi:10.1021/es00142a004, 1985

560   Conrad, R., Meyer, O., & Seiler, W.: Role of carboxydobacteria in consumption of atmospheric carbon

561   monoxide by soil, Applied and Environmental Microbiology, 42(2), 211–215, 1981

562   Crutzen, P. J., & Giedel, L. T.: A two-dimensional photochemical model of the atmosphere. 2: The

563   tropospheric budgets of anthropogenic chlorocarbons CO, CH4, CH3Cl and the effect of various NOx

564   sources on tropospheric ozone, J. Geophys. Res., 88(Cll), 6641–6661. doi:10.1029/JC088iC11p06641,

565   1983

566   Crutzen, P.J.: Role of the tropics in atmospheric chemistry, The Geophysiology of Amazonia Vegetation

567   Climate Interaction (Dickinson RE, ed.), pp 107–131. John Wiley, New York, 1987

568   Daniel, J. S., & Solomon, S.: On the climate forcing of carbon monoxide, Journal of Geophysical Research-

569   Atmospheres, 103(D11), 13249–13260. doi:10.1029/98JD00822, 1988

570   Dee, D. P., Uppala, S. M., Simmons, A. J., Berrisford, P., Poli, P., Kobayashi, S., … Vitart, F.: The ERA-

571   Interim reanalysis: configuration and performance of the data assimilation system, Quarterly Journal of the

572   Royal Meteorological Society, doi:10.1002/qj.828, 2011

573   Dentener, F., Drevet, J., Lamarque, J. F., Bey, I., Eickhout, B., Fiore, A. M., … Wild, O.: Nitrogen and sulfur

574   deposition on regional and global scales: A multimodel evaluation, Global Biogeochemical Cycles, 20(4),

575   doi:10.1029/2005GB002672, 2006

576   Derendorp, L., Quist, J. B., Holzinger, R., & Röckmann, T.: Emissions of H2 and CO from leaf litter of

577   Sequoiadendron giganteum, and their dependence on UV radiation and temperature, Atmospheric

578   Environment, 45(39), 7520–7524. doi:10.1016/j.atmosenv.2011.09.044, 2011

579   Duan, Q. Y., Gupta, V. K., & Sorooshian, S.: Shuffled complex evolution approach for effective and efficient

580   global minimization, Journal of Optimization Theory and Applications, 76(3), 501–521.

581   doi:10.1007/BF00939380, 1993

582   Duggin, J. A., & Cataldo, D. A.: The rapid oxidation of atmospheric CO to CO2 by soils, Soil Biology and

583   Biochemistry, 17(4), 469–474, doi:10.1016/0038-0717(85)90011-2, 1985

584   Emmons, L. K., Walters, S., Hess, P. G., Lamarque, J.-F., Pfister, G. G., Fillmore, D., … Kloster, S.:

585   Description and evaluation of the Model for Ozone and Related chemical Tracers, version 4 (MOZART-

586   4), Geoscientific Model Development, 3(1), 43–67. doi:10.5194/gmd-3-43-2010, 2010

587   Fenchel, T., King, G. M., & Blackburn, T. H.: Bacterial biogeochemistry: the ecophysiology of mineral

588   cycling, Bacterial biogeochemistry (p. 307 pp). doi:10.1016/B978-0-12-415836-8.00012-8, 1988

589   Ferenci, T., Strom, T., & Quayle, J. R.: Oxidation of carbon monoxide and methane by Pseudomonas

590   methanica, Journal of General Microbiology, 91(1), 79–91. doi:10.1099/00221287-91-1-79, 1975

591   Fisher, M. E.: Soil-atmosphere Exchange of Carbon Monoxide in Forest Stands Exposed to Elevated and

592   Ambient CO2 (Doctoral dissertation), 2003

593 Fraser, W. T., Blei, E., Fry, S. C., Newman, M. F., Reay, D. S., Smith, K. A., & McLeod, A. R.: Emission of
594 methane, carbon monoxide, carbon dioxide and short-chain hydrocarbons from vegetation foliage under
595 ultraviolet irradiation, Plant, Cell and Environment, 38(5), 980–989. doi:10.1111/pce.12489, 2015

596 Funk, D. W., Pullman, E. R., Peterson, K. M., Crill, P. M., & Billings, W. D.: Influence of water table on
597 carbon dioxide, carbon monoxide, and methane fluxes from Taiga Bog microcosms, Global Biogeochem.
598 Cycles, 8(3), 271–278. doi:10.1029/94gb0122, 1994

599 Galbally, I., Meyer, C. P., Wang, Y. P., & Kirstine, W.: Soil-atmosphere exchange of CH4, CO, N2O and
600 NOx and the effects of land-use change in the semiarid Mallee system in Southeastern Australia, Global
601 Change Biology, 16(9), 2407–2419, doi:10.1111/j.1365-2486.2010.02161.x, 2010

602 Gille, J.: MOPITT Gridded Monthly CO Retrievals (Near and Thermal Infrared Radiances) - Version 6 [Data
603 set], NASA Langley Atmospheric Science Data Center. doi:10.5067/TERRA/MOPITT/DATA301, 2013

604 Gödde, M., Meuser, K., & Conrad, R.: Hydrogen consumption and carbon monoxide production in soils with
605 different properties, Biology and Fertility of Soils, 32(2), 129–134, doi:10.1007/s003740000226, 2000

606 Guthrie, P. D.: The CH4- CO - OH conundrum: A simple analytic approach, Global Biogeochemical Cycles,
607 doi:10.1029/gb003i004p00287, 1989

608 Hardy, K. R., & King, G. M.: Enrichment of High-Affinity CO Oxidizers in Maine Forest Soil. Applied and
609 Environmental Microbiology, 67(8), 3671–3676, doi:10.1128/AEM.67.8.3671-3676.2001, 2001

610 Harris, I., Jones, P. D., Osborn, T. J., & Lister, D. H.: Updated high-resolution grids of monthly climatic
611 observations - the CRU TS3.10 Dataset, International Journal of Climatology, doi:10.1002/joc.3711, 2013

612 He, H., & He, L.: The role of carbon monoxide signaling in the responses of plants to abiotic stresses, Nitric
613 Oxide : Biology and Chemistry / Official Journal of the Nitric Oxide Society, 42, 40–3.
614 doi:10.1016/j.niox.2014.08.011, 2014

615 Heichel, G. H.: Removal of Carbon Monoxide by Field and Forest Soils1, Journal of Environment Quality,
616 American Society of Agronomy, doi:10.2134/jeq1973.00472425000200040001x, 1973

617 Jobbagy, E. G., & Jackson, R.: The vertical Distribution of soil organic carbon and its relation to climate and
618 vegetation, Ecological Applications, 10:2(April), 423–436, doi:10.2307/2641104, 2000

619 Jones, R. D., & Morita, R. Y.: Carbon monoxide oxidation by chemolithotrophic ammonium
620 oxidizers, Canadian Journal of Microbiology, 29(11), 1545–1551, doi:10.1139/m83-237, 1983

621 Khalil, M. A. ., Pinto, J. ., & Shearer, M.: Atmospheric carbon monoxide, Chemosphere - Global Change
622 Science, Elsevier BV, doi:s1465-9972(99)00053-7,1999

623 Khalil, M. A. K., & Rasmussen, R. A.: The global cycle of carbon monoxide: Trends and mass
624 balance, Chemosphere, 20(1–2), 227–242, doi:10.1016/0045-6535(90)90098-E, 1990

625 King, G. M.: Attributes of Atmospheric Carbon Monoxide Oxidation by Maine Forest Soils, Appl. Environ.
626 Microbiol., 65(12), 5257–5264, 1999

627 King, G. M.: Characteristics and significance of atmospheric carbon monoxide consumption by soils,
628 Chemosphere, 1, 53–63, doi:10.1016/S1465-9972(99)00021-5, 1999a

629   King, G. M.: Land use impacts on atmospheric carbon monoxide consumption by soils, Global
630   Biogeochemical Cycles, 14(4), 1161–1172, doi:10.1029/2000GB001272, 2000

631   King, G. M., & Crosby, H.: Impacts of plant roots on soil CO cycling and soil-atmosphere CO
632   exchange, Global Change Biology, 8(11), 1085–1093, doi:10.1046/j.1365-2486.2002.00545.x, 2002

633   King, G. M., & Hungria, M.: Soil-atmosphere CO exchanges and microbial biogeochemistry of CO
634   transformations in a Brazilian agricultural ecosystem, Applied and Environmental Microbiology, 68(9),
635   4480–4485, doi:10.1128/AEM.68.9.4480-4485.2002, 2002

636   King, G. M., & Weber, C. F.: Distribution, diversity and ecology of aerobic CO-oxidizing bacteria, Nature
637   Reviews, Microbiology, 5(2), 107–18, doi:10.1038/nrmicro1595, 2007

638   King, J. Y., Brandt, L. A., & Adair, E. C.: Shedding light on plant litter decomposition: advances, implications
639   and new directions in understanding the role of photodegradation, Biogeochemistry, 111(1–3), 57–81,
640   doi:10.1007/s10533-012-9737-9, 2012

641   Kisselle, K. W., Zepp, R. G., Burke, R. A., De Pinto, A. S., Bustamante, M. M. C., Opsahl, S., … Viana, L.
642   T.: Seasonal soil fluxes of carbon monoxide in burned and unburned Brazilian savannas, Journal of
643   Geophysical Research Atmospheres, 107(20), doi:10.1029/2001JD000638, 2002

644   Kuhlbusch, T. A., Zepp, R. G., Miller, W. L., & A BURKE, R.: Carbon monoxide fluxes of different soil layers
645   in upland Canadian boreal forests, Tellus B. Informa UK Limited, doi:10.1034/j.1600-0889.1998.t01-3-
646   00003.x, 1998

647   Lamarque, J. F., Emmons, L. K., Hess, P. G., Kinnison, D. E., Tilmes, S., Vitt, F., … Tyndall, G. K.: CAM-
648   chem: Description and evaluation of interactive atmospheric chemistry in the Community Earth System
649   Model, Geoscientific Model Development, 5(2), 369–411, https://doi.org/10.5194/gmd-5-369-2012, 2012

650   Lee, H., Rahn, T., & Throop, H.: An accounting of C-based trace gas release during abiotic plant litter
651   degradation, Global Change Biology, 18(3), 1185–1195, doi:10.1111/j.1365-2486.2011.02579.x, 2012

652   Logan, J. A., Prather, M. J., Wofsy, S. C., & McElroy, M. B.: Tropospheric chemistry - A global perspective, J.
653   Geophys. Res., doi:10.1029/JC086iC08p07210, 1981

654   Lu, Y., & Khalil, M. A. K.: Methane and carbon monoxide in OH chemistry: The effects of feedbacks and
655   reservoirs generated by the reactive products, Chemosphere. Elsevier BV, doi:10.1016/0045-
656   6535(93)90450-j, 1993

657   Luo, M., Read, W., Kulawik, S., Worden, J., Livesey, N., Bowman, K., & Herman, R.: Carbon monoxide
658   (CO) vertical profiles derived from joined TES and MLS measurements, Journal of Geophysical Research
659   Atmospheres, 118(18), 10601–10613, doi:10.1002/jgrd.50800, 2013

660   Moxley, J. M., & Smith, K. A.: Factors affecting utilisation of atmospheric CO by soils, Soil Biology and
661   Biochemistry, 30(1), 65–79, doi:10.1016/S0038-0717(97)00095-3, 1998

662   Myhre, G., Shindell, D., Bréon, F. M., Collins, W., Fuglestvedt, J., Huang, J., ... & Nakajima, T.:
663   Anthropogenic and Natural Radiative Forcing. In: Climate Change 2013: The Physical Science Basis,

Contribution of Working Group 1 to the Fifth Assessment Report of the Intergovernmental Panel on Climate Change. Table, 8, 714, 2013

Nakai, T., Kim, Y., Busey, R. C., Suzuki, R., Nagai, S., Kobayashi, H., … Ito, A.: Characteristics of evapotranspiration from a permafrost black spruce forest in interior Alaska. Polar Science, 7(2), 136–148. doi:10.1016/j.polar.2013.03.003, 2013

Philip, R., & Novick, K.: AmeriFlux US-MMS Morgan Monroe State Forest [Data set]. AmeriFlux; Indiana University, doi:10.17190/AMF/1246080, 2016

Pihlatie, M., Rannik, Ü., Haapanala, S., Peltola, O., Shurpali, N., Martikainen, P. J., … Mammarella, I.: Seasonal and diurnal variation in CO fluxes from an agricultural bioenergy crop, Biogeosciences. Copernicus GmbH, doi:10.5194/bg-13-5471-2016, 2016

Potter, C. S., Klooster, S. A., & Chatfield, R. B.: Consumption and production of carbon monoxide in soils: A global model analysis of spatial and seasonal variation, Chemosphere, 33(6), 1175–1193, doi:10.1016/0045-6535(96)00254-8, 1996

Prather, M., and Ehhalt, D.: Atmospheric chemistry and greenhouse gases. Climate Change, 2001: The Scientific Basis (Houghton JT, Ding Y, Griggs DJ, Noguer M, van der Linden PJ, Dai X, Maskell K & Johnson CA, eds), pp. 239–288, Cambridge University Press, Cambridge, UK, 2001

Prather, M., Derwent, R., Ehhalt, D., Fraser, P., Sanheeza, E. and Zhou, X.: Other trace gases and atmospheric chemistry, Climate Change, 1994. Radiative Forcing of Climate Change (Houghton JT, Meira Filho LG, Bruce J, Hoesung Lee BA, Callander E, Haites E, Harris N & Maskell K, eds), pp. 76–126, Cambridge University Press, Cambridge, UK, 1995

SALESKA, S. R., DA ROCHA, H. R., HUETE, A. R., NOBRE, A. D., ARTAXO, P. E., & SHIMABUKURO, Y. E.: LBA-ECO CD-32 Flux Tower Network Data Compilation, Brazilian Amazon: 1999-2006, ORNL Distributed Active Archive Center, doi:10.3334/ORNLDAAC/1174, 2013

Sanderson, M. G., Collins, W. J., Derwent, R. G., & Johnson, C. E.: Simulation of global hydrogen levels using a Lagrangian three-dimensional model, Journal of Atmospheric Chemistry, 46(1), 15–28, doi:10.1023/A:1024824223232, 2003

Sanhueza, E., Dong, Y., Scharffe, D., Lobert, J. M., & Crutzen, P. J.: Carbon monoxide uptake by temperate forest soils: The effects of leaves and humus layers, Tellus, Series B: Chemical and Physical Meteorology, 50(1), 51–58, doi:10.1034/j.1600-0889.1998.00004.x, 1998

Schade, G. W., & Crutzen, P. J.: CO emissions from degrading plant matter (II). Estimate of a global source strength, Tellus, Series B: Chemical and Physical Meteorology, 51(5), 909–918, doi:10.1034/j.1600-0889.1999.t01-4-00004.x, 1999

Scharffe, D., Hao, W. M., Donoso, L., Crutzen, P. J., & Sanhueza, E.: Soil fluxes and atmospheric concentration of CO and CH4 in the northern part of the Guayana shield, Venezuela, Journal of Geophysical Research-Atmospheres, 95(90), 22475–22480, doi:10.1029/JD095iD13p22475, 1990

Seiler, W.: In: Krumbein, W.E. (Ed.), Environmental Biogeochemistry and Geomicrobiology, Methods, Metals and Assessment, vol. 3, Ann Arbor Science, Ann Arbor, MI, pp. 773-810, 1987

Seinfeld, J. H., & Pandis, S. N.: Atmospheric Chemistry and Physics: From Air Pollution to Climate Change, Atmospheric Chemistry and Physics from Air Pollution to Climate Change Publisher New York NY Wiley 1998 Physical Description Xxvii 1326 p A WileyInterscience Publication ISBN 0471178152, 51, 1–4, doi:10.1080/00139157.1999.10544295, 1998

Stein, O., Schultz, M. G., Bouarar, I., Clark, H., Huijnen, V., Gaudel, A., … Clerbaux, C.: On the wintertime low bias of Northern Hemisphere carbon monoxide found in global model simulations, Atmospheric Chemistry and Physics, 14(17), 9295–9316, doi:10.5194/acp-14-9295-2014, 2014

Stevenson, D. S., Dentener, F. J., Schultz, M. G., Ellingsen, K., van Noije, T. P. C., Wild, O., … Szopa, S.: Multimodel ensemble simulations of present-day and near-future tropospheric ozone, Journal of Geophysical Research Atmospheres, 111(8), doi:10.1029/2005JD006338, 2006

Suzuki, R.: AmeriFlux US-Prr Poker Flat Research Range Black Spruce Forest [Data set], AmeriFlux; Japan Agency for Marine-Earth Science and Technology, doi:10.17190/AMF/1246153, 2016

Tan, Z., & Zhuang, Q.: An analysis of atmospheric CH_4 concentrations from 1984 to 2008 with a single box atmospheric chemistry model, Atmospheric Chemistry and Physics Discussions, Copernicus GmbH, doi:10.5194/acpd-12-30259-2012, 2012

Tarr, M. a., Miller, W. L., & Zepp, R. G.: Direct carbon monoxide photoproduction from plant matter, Journal of Geophysical Research, 100, 11403, doi:10.1029/94JD03324, 1995

Taylor, J. A., Zimmerman, P. R., & Erickson, D. J.: A 3-D modelling study of the sources and sinks of atmospheric carbon monoxide, Ecological Modelling, 88(1–3), 53–71, doi:10.1016/0304-3800(95)00069-0, 1996

van Asperen, H., Warneke, T., Sabbatini, S., Nicolini, G., Papale, D., & Notholt, J.: The role of photo- and thermal degradation for CO_2 and CO fluxes in an arid ecosystem, Biogeosciences, 12(13), 4161–4174, doi:10.5194/bg-12-4161-2015, 2015

Varella, R. F., Bustamante, M. M. C., Pinto, A. S., Kisselle, K. W., Santos, R. V., Burke, R. A., … Viana, L. T.: Soil fluxes of CO2, CO, NO, and N2O from an old pasture and from native Savanna in Brazil, Ecological Applications, 14(4 SUPPL.), doi:10.1890/01-6014, 2004

Vreman, H. J., Wong, R. J., & Stevenson, D. K.: Quantitating carbon monoxide production from heme by vascular plant preparations in vitro, Plant Physiology and Biochemistry, 49(1), 61–68, doi:10.1016/j.plaphy.2010.09.021, 2011

Wesely, M. L.: Parameterization of surface resistances to gaseous dry deposition in regional-scale numerical models. Atmospheric Environment (1967), Elsevier BV, doi:10.1016/0004-6981(89)90153-4, 1989

Wesely, M., & Hicks, B.: A review of the current status of knowledge on dry deposition. Atmospheric Environment, 34, 2261–2282, doi:10.1016/S1352-2310(99)00467-7, 2000

Whalen, S. C., & Reeburgh, W. S.: Carbon monoxide consumption in upland boreal forest soils, Soil Biology and Biochemistry, 33(10), 1329–1338, doi:10.1016/S0038-0717(01)00038-4, 2001

737 Yonemura, S., Kawashima, S., & Tsuruta, H.: Carbon monoxide, hydrogen, and methane uptake by soils

738 in a temperate arable field and a forest, Journal of Geophysical Research, 105(Dll), 14347,

739 https://doi.org/10.1029/1999JD901156, 2000

740 Yoon, J., & Pozzer, A.: Model-simulated trend of surface carbon monoxide for the 2001-2010

741 decade, Atmospheric Chemistry and Physics, 14(19), 10465–10482, doi:10.5194/acp-14-10465-2014,

742 2014

743 Zepp, R. G., Miller, W. L., Tarr, M. A., Burke, R. A., & Stocks, B. J.: Soil-atmosphere fluxes of carbon

744 monoxide during early stages of postfire succession in upland Canadian boreal forests, Journal of

745 Geophysical Research-Atmospheres, 102(D24), 29301–29311, doi:10.1029/97jd01326, 1997

746 Zhuang, Q., McGuire, A. D., Melillo, J. M., Clein, J. S., Dargaville, R. J., Kicklighter, D. W., … Hobbie, J. E.:

747 Carbon cycling in extratropical terrestrial ecosystems of the Northern Hemisphere during the 20th century:

748 A modeling analysis of the influences of soil thermal dynamics, Tellus, Series B: Chemical and Physical

749 Meteorology, 55(3), 751–776, doi:10.1034/j.1600-0889.2003.00060.x, 2003

750 Zhuang, Q., Melillo, J. M., Kicklighter, D. W., Prinn, R. G., McGuire, A. D., Steudler, P. A., … Hu, S.:

751 Methane fluxes between terrestrial ecosystems and the atmosphere at northern high latitudes during the

752 past century: A retrospective analysis with a process-based biogeochemistry model, Global

753 Biogeochemical Cycles, 18(3), doi:10.1029/2004GB002239, 2004

754 Zhuang, Q., Melillo, J. M., McGuire, A. D., Kicklighter, D. W., Prinn, R. G., Steudler, P. A., … Hu, S.: Net

755 emissions of CH4 and CO2 in Alaska: Implications for the region's greenhouse gas budget, Ecological

756 Applications, 17(1), 203–212, doi:10.1890/1051-0761(2007)017[0203:NEOCAC]2.0.CO;2, 2007

757 Zhuang, Q., Romanovsky, V. E., & McGuire, a. D.: Incorporation of a permafrost model into a large-scale

758 ecosystem model: Evaluation of temporal and spatial scaling issues in simulating soil thermal

759 dynamics, Journal of Geophysical Research, 106, 33649, doi:10.1029/2001JD900151, 2001

760 Zhuang, Q., Chen, M., Xu, K., Tang, J., Saikawa, E., Lu, Y., … McGuire, A. D.: Response of global soil

761 consumption of atmospheric methane to changes in atmospheric climate and nitrogen deposition, Global

762 Biogeochemical Cycles, doi:10.1002/gbc.20057, 2013

763 **Table 1.** Model parameterization sites for the thermal and hydrology modules (site No. 1-4) and for the CODM module (site No. 5-13)

No.	Site Name	Location	Vegetation	Driving Climate	Observed Data	Source and Comments
1	Poker Flat Research Range Black Spruce Forest (US_PRR)	147°29'W/65°7'N	Boreal Evergreen Needle Leaf Forests	Site Observation & ERA Interim	Soil Temperature and Moisutre of 2011-2014	Suzuki (2016)
2	Morgan Monroe State Forest (US_MMS)	86°25W/39°19'N	Temperate Deciduous Broadleaf Forests	Site Observation & ERA Interim	Soil Temperature and Moisutre of 1999-2014	Philip and Novick (2016)
3	Santarem, Tapajos National Forest (STM_K83)	54°56'W/3°3'S	Tropical Moist Forest	Site Observation & ERA Interim	Soil Temperature and Moisutre of 2000-2004	SALESKA et al. (2013)
4	Bananal Island Site (TOC_BAN)	50°08'W/9°49'S	Tropical Forest-Savanna	Site Observation & ERA Interim	Soil Temperature and Moisutre of 2003-2006	SALESKA et al. (2013)
5	Eastern Finland (EF)	27°14E/63°9'N	Boreal Grassland	Site Observation & ERA Interim	CO flux of April-November,2011	Pihlatie et.al. (2016)
6	Viterbo, Italy (VI)	11°55'E/42°22'N	Mediterranean Grassland	Site Observation & ERA Interim	CO flux of August, 2013	van Asperen et al. (2015)
7	Brasilia, Brazil (BB)	47°51'W/15°56'S	Tropical Savanna	Site Observation & CRU	CO flux of October 1999 to July 2001	Varella et al. (2004)
8	Orange County, North Carolina (OC)	79°7'W/35°58'N	Temperate Coniferous Forest	AMF_US-Dk3 2002-2003	CO flux of March 2002 to March 2003	Fisher (2003)
9	Tsukuba Science City, Japan (TSC)	140°7'E/36°01'N	Temperate Mixed Forest	Site Observation & ERA Interim	CO flux of July 1996 to September 1997	Yonemura et. al. (2000)
10	Manitoba, Canada (CBS)	96°44'W/56°09'N	Boreal Pine Forest	Site Observation & AMF_CA-Man	CO flux of June-August, 1994	Kuhlbusch et. al (1998)
11	Scotland, U.K. (SUK)	3°12'W/55°51'N	Temperate Deciduous Forests	ERA Interim 1995	CO flux of 1995	Moxley and Smith (1998)
12	Alaska, USA (AUS)	147°41'W/64°52'N	Boreal wetland	CRU 1991	CO flux of Lab Experiment,1991	Funk et al. (1994)
13	Guayana Shield,Bolivar State,Venezuela (GBV)	62°57'W/7°51'N	Tropical Smideciduous Forest	CRU 1985	CO flux of Lab Experiment,1985	Scharffe et al. (1990)

764

765

766 **Table 2.** Ecosystem-specific parameters in the CODM module[a]

	Ecosystem Type	k_{CO} (ul CO l^{-1})	$Vmax$ (ug CO $g^{-1}h^{-1}$)	T_{ref} (°C)	$Q10$ (Unitless)	M_{min} ($\frac{v}{v}$)	M_{max} ($\frac{v}{v}$)	M_{opt} ($\frac{v}{v}$)	E_{SOC}	F_{SOC} ($\frac{g}{g}$)	$\frac{Ea_{ref}}{R}$ (K)	PM_{ref} ($\frac{v}{v}$)	PT_{ref} (°C)
1	Alpine Tundra & Polar Desert	36.00	0.78	4.00	1.80	0.10	1.00	0.55	3.00	0.33	7700	0.25	30.00
2	Wet Tundra	36.00	0.70	4.00	1.80	0.25	1.00	0.55	3.00	0.42	7700	0.25	30.00
3	Boreal Forest	27.34	1.18	9.81	1.60	0.15	0.64	0.53	2.98	0.50	8827	0.35	26.99
4	Temperate Coniferous Forest	42.64	2.15	6.90	1.87	0.02	0.96	0.53	2.86	0.50	8404	0.38	31.52
5	Temperate Deciduous Forest	40.16	2.43	8.54	1.51	0.17	0.81	0.51	2.45	0.50	8801	0.35	37.44
6	Grassland	42.41	0.49	11.27	1.65	0.16	0.82	0.51	3.09	0.42	14165	0.24	12.29
7	Xeric Shrublands	8.00	0.30	4.00	1.50	0.10	1.00	0.55	3.00	0.33	7700	0.25	30.00
8	Tropical Forest	45.00	2.00	4.00	1.50	0.10	1.00	0.55	3.80	0.50	14000	0.50	18.00
9	Xeric Woodland	8.00	0.30	4.00	1.50	0.10	1.00	0.55	3.00	0.50	7700	0.25	30.00
10	Temperate Evergreen Broadleaf Forest	40.16	2.43	8.54	1.51	0.17	0.81	0.51	2.45	0.50	8801	0.35	37.44
11	Mediterranean Shrubland	45.00	1.50	4.00	1.50	0.10	1.00	0.55	3.00	0.33	7700	0.25	30.00
**	Largest Potential Value	51.00	11.1	15.00	2.00	0.30	1.00	0.60	3.80	--	15000	0.60	40.00

767
768 [a] k_{CO} is the half-saturation constant for soil CO concentration; $Vmax$ is the specific maximum CO oxidation rate; T_{ref} is the reference temperature to account for the soil temperature effects on the CO consumption; $Q10$ is the an ecosystem-specific Q10 coefficient to account for soil temperature effects on the CO consumption; M_{min}, M_{max}, M_{opt} are the minimum, optimum, and maximum volumetric soil moistures of oxidation reaction to account for soil moisture effects on the CO consumption; E_{SOC} is an estimated nominal CO production factor, similar as Potter et al. (1996) (10^{-4} mg CO m^{-2} d^{-1} per g SOC m^{-2}); F_{SOC} is a constant fraction of top 20cm SOC compared to total amount of SOC to account for SOC effects on the CO production; Ea_{ref}/R is the is the ecosystem-specific activation energy divided by gas constant to account for the reaction rate of production; PM_{ref} is the reference moisture to account for soil temperature effects on the CO production; PT_{ref} is the reference temperature to account for soil temperature effects on the CO production

769 **Table 3.** Regional soil CO consumption, net flux and production (Tg CO yr^{-1}) during 2000-2013

	South-45S	45S-0	0-45N	45N-North	Global
Consumption	0.22	75.77	91.66	18.90	186.55
Net flux	0.13	59.34	77.17	14.63	151.27
Production	0.09	16.43	14.49	4.27	35.28

770

771

Table 4. Annual total soil CO consumption, net flux and production in different ecosystems during 2000-2013 (E1) and mean CO deposition velocity in different ecosystems during 1901-2013 (E2)

Vegetation Type	Area (10^6 km^2)	Pixels	Consumption (Tg CO yr^{-1})	Net flux (Tg CO yr^{-1})	Production (Tg CO yr^{-1})	Deposition velocity (mm s^{-1})
Alpine Tundra & Polar Desert	5.28	3580	-0.92	-0.69	0.23	0.023
Wet Tundra	5.24	4212	-1.00	-0.42	0.58	0.015
Boreal Forest	12.47	7578	-7.76	-6.01	1.75	0.070
Forested Boreal Wetland	0.23	130	-0.14	-0.09	0.04	0.109
Boreal Woodland	6.48	4545	-2.48	-1.54	0.94	0.036
Non-Forested Boreal Wetland	0.83	623	-0.35	-0.18	0.17	0.029
Mixed Temperate Forest	5.25	2320	-10.49	-9.98	0.51	0.204
Temperate Coniferous Forest	2.49	1127	-3.51	-3.21	0.30	0.185
Temperate Deciduous Forests	3.65	1666	-5.07	-4.83	0.25	0.151
Temperate Forested Wetland	0.15	60	-0.35	-0.35	0.01	0.281
Tall Grassland	3.63	1567	-1.66	-0.65	1.01	0.021
Short Grassland	4.71	2072	-1.05	-0.27	0.78	0.010
Tropical Savanna	13.85	4666	-21.86	-15.88	5.98	0.234
Xeric Shrubland	14.71	5784	-1.95	-1.64	0.31	0.021
Tropical Evergreen Forest	17.77	5855	-85.90	-69.66	16.24	0.879
Tropical Forested Wetland	0.55	178	-3.59	-3.09	0.50	1.154
Tropical Deciduous Forest	4.69	1606	-14.81	-11.78	3.03	0.532
Xeric Woodland	6.85	2387	-8.48	-7.44	1.04	0.246
Tropical Forested Floodplain	0.15	50	-0.89	-0.77	0.12	1.117
Desert	11.61	4170	-0.62	-0.57	0.05	0.008
Tropical Non-forested Wetland	0.06	19	-0.03	-0.02	0.01	0.067
Tropical Non-forested Floodplain	0.36	120	-0.35	-0.24	0.10	0.083
Temperate Non-Forested Weland	0.34	120	-0.33	-0.20	0.14	0.089
Temperate Forested Floodplain	0.10	48	-0.13	-0.12	0.00	0.197
Temperate Non-forested Floodplain	0.10	45	-0.05	-0.03	0.02	0.050
Wet Savanna	0.16	59	-0.39	-0.32	0.07	0.434
Salt Marsh	0.09	35	-0.05	-0.03	0.03	0.035
Mangroves	0.12	38	-0.49	-0.41	0.08	0.809
Temperate Savannas	6.83	2921	-3.83	-3.22	0.61	0.076
Temperate Evergreen Broadleaf	3.33	1268	-7.17	-6.95	0.22	0.252
Mediterranean Shrubland	1.47	575	-0.86	-0.71	0.16	0.100
Total	133.56	59424	-186.55	-151.27	35.28	--

779

Table 5. Sensitivity of the global CO consumption, net flux and production (Tg CO yr^{-1}) to the changes in

atmospheric CO, soil organic carbon (SOC), precipitation (Prec) and air temperature (AT)

	Baseline	CO +30%	CO -30%	SOC +5%	SOC -5%	Prec +30%	Prec -30%	AT +3°C	AT -3°C
Consumption	-147.65	-164.14	-131.12	-152.27	-143.03	-150.72	-143.50	-190.59	-114.83
Change (%)	0.00	11.17	-11.19	3.13	-3.13	2.08	-2.81	29.09	-22.23
Net flux	-113.65	-130.15	-97.12	-116.58	-110.73	-116.97	-109.32	-144.23	-89.58
Change (%)	0.00	14.51	-14.54	2.57	-2.57	2.92	-3.81	26.90	-21.18
Production	33.99	33.99	33.99	35.69	32.29	33.74	34.17	46.36	25.25
Change (%)	0.00	0.00	0.00	5.00	-5.00	-0.75	0.53	36.39	-25.72

782

783

784

785

786

787

788

789

790

791

792

793

794

795

796

797

798

799

800

801 **Table 6.** Correlation coefficients between forcing variables (precipitation (Prec), air temperature (Tair), soil

802 organic carbon (SOC), soil temperature (Tsoil), soil moisture (Msoil) and atmospheric CO (CO air)) and absolute

803 values of consumption, production and net flux for different regions and the globe

		Monthly					Annual				
		North-45°N	45°N-0°	0°-45°S	45°S-South	Global	North-45°N	45°N-0°	0°-45°S	45°S-South	Global
Prec	Consumption	0.91	0.96	0.92	-0.34	0.87	0.65	0.21	0.26	0.13	0.52
	Production	0.91	0.70	0.45	-0.34	0.82	0.63	0.10	0.15	-0.11	0.47
	Net flux	0.91	0.97	0.94	-0.33	0.87	0.65	0.25	0.31	0.32	0.54
Tair	Consumption	0.97	0.98	0.91	0.96	0.95	0.92	0.93	0.88	0.84	0.91
	Production	0.96	0.83	0.72	0.98	0.94	0.92	0.92	0.91	0.95	0.91
	Net Flux	0.97	0.97	0.88	0.90	0.95	0.91	0.92	0.85	0.62	0.91
SOC	Consumption	-0.19	0.07	0.21	-0.01	0.15	0.68	0.90	0.92	0.47	0.92
	Production	-0.19	0.31	0.47	-0.02	0.24	0.72	0.92	0.92	0.50	0.93
	Net Flux	-0.19	0.03	0.14	0.00	0.13	0.67	0.88	0.91	0.38	0.91
Tsoil	Consumption	0.97	0.98	0.92	0.96	0.95	0.94	0.93	0.88	0.85	0.95
	Production	0.97	0.83	0.72	0.98	0.94	0.94	0.92	0.91	0.96	0.95
	Net Flux	0.98	0.97	0.88	0.90	0.95	0.93	0.93	0.86	0.63	0.95
Msoil	Consumption	0.85	0.96	0.92	0.19	0.76	0.03	0.22	0.14	0.26	0.22
	Production	0.85	0.75	0.44	0.14	0.69	-0.02	0.12	0.02	0.05	0.17
	Net Flux	0.84	0.96	0.95	0.25	0.77	0.04	0.26	0.19	0.40	0.24
CO Air	Consumption	-0.66	-0.76	-0.29	0.14	-0.48	0.87	0.88	0.81	0.98	0.91
	Production	-0.70	-0.66	0.08	-0.40	-0.66	-0.36	-0.48	-0.54	-0.44	-0.57
	Net Flux	-0.64	-0.73	-0.35	0.55	-0.41	0.92	0.91	0.88	0.99	0.94

804

805

806

807

808

809

810

811

812

813

814

815
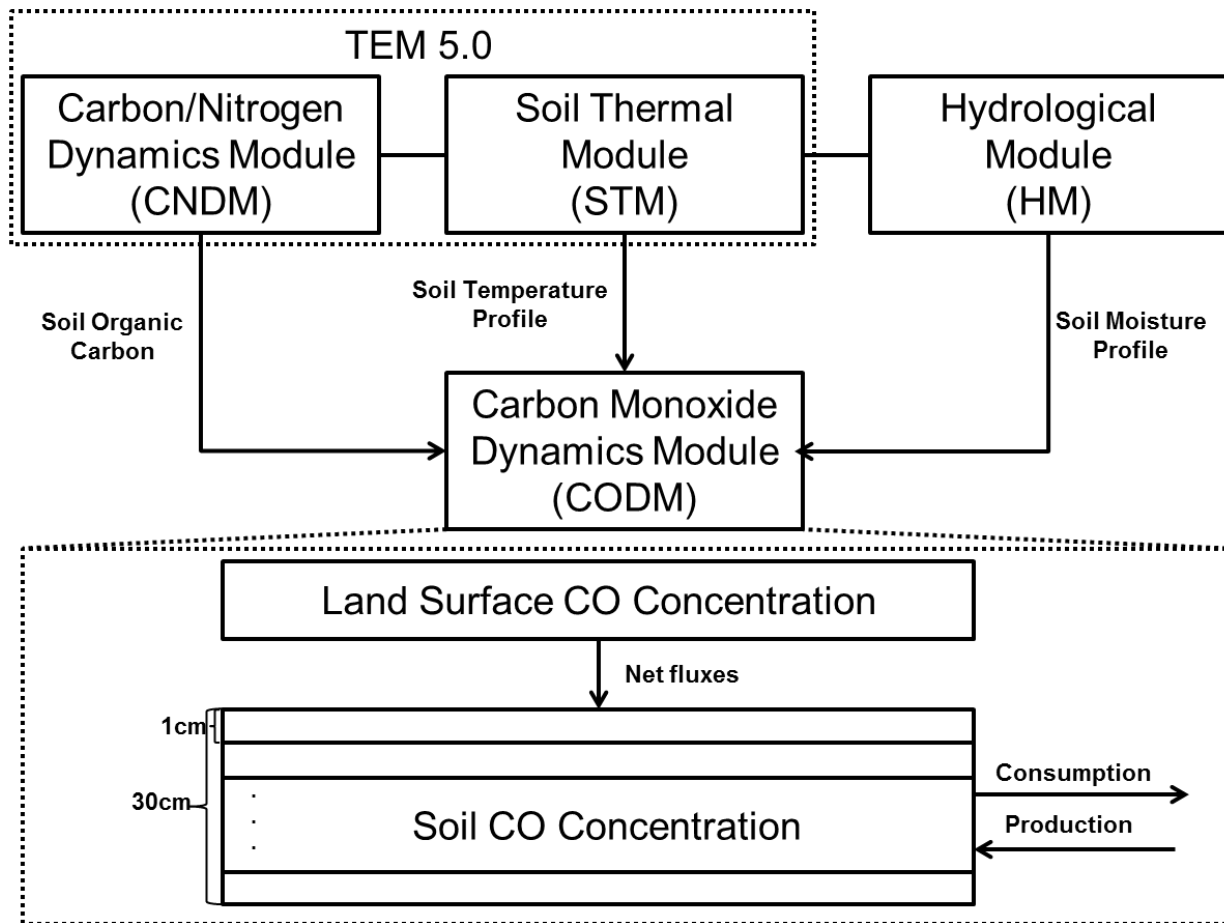
Figure 1. The model framework includes a carbon and nitrogen dynamics module (CNDM), a soil thermal module (STM) from Terrestrial Ecosystem Model (TEM) 5.0 (Zhuang et al., 2001, 2003), a hydrological module (HM) based on a Land Surface Module (Bonan, 1996; Zhuang et al., 2004), and a carbon monoxide dynamics module (CODM). The detailed structure of CODM includes land surface CO concentration as top boundary and thirty 1 cm thick layers (totally 30 cm) where consumption and production take place.

821

822

823

824

825
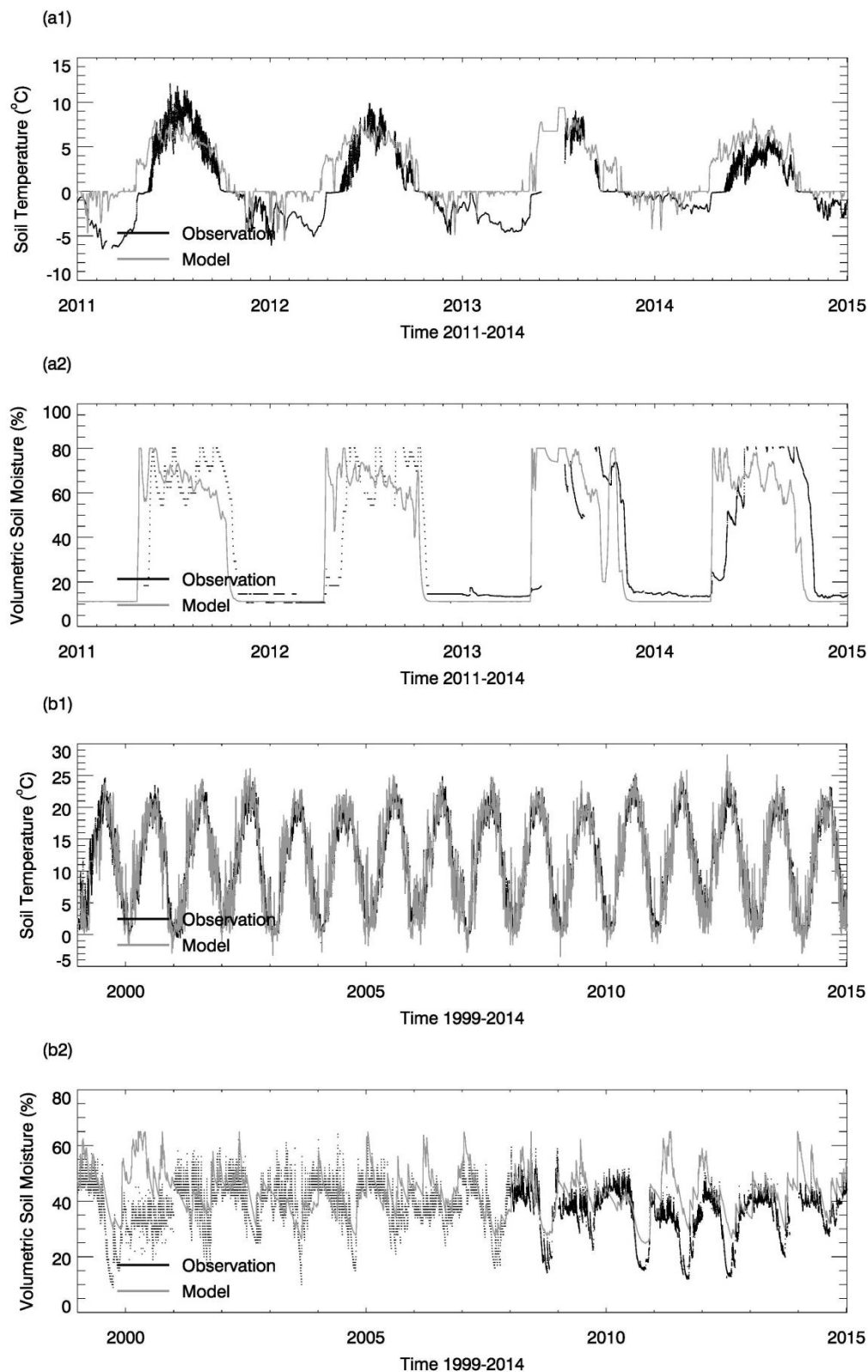
Figure 2. Evaluation of thermal and hydrology module at four sites: (a) Boreal Evergreen Needle Leaf Forests, (b) Temperate Deciduous Broadleaf Forests. (1) shows the soil temperature comparison between the model simulations (gray line) and observations (black line) and (2) shows the soil moisture comparison between the model simulations (gray line) and observations (black line). Specifically, the volumetric soil moisture is converted from the water content reflectometry (WCR) probe output period using an empirical calibration function of Bourgeau-Chavez et al. (2012) for 5cm-30cm layer. Some of them resulted in calculations of values greater than 100% VSM in Nakai et al. (2013) study. Our model estimated high VSM (close to 80%) is due to top 10 cm moss in the model which has a saturation VSM of 0.8
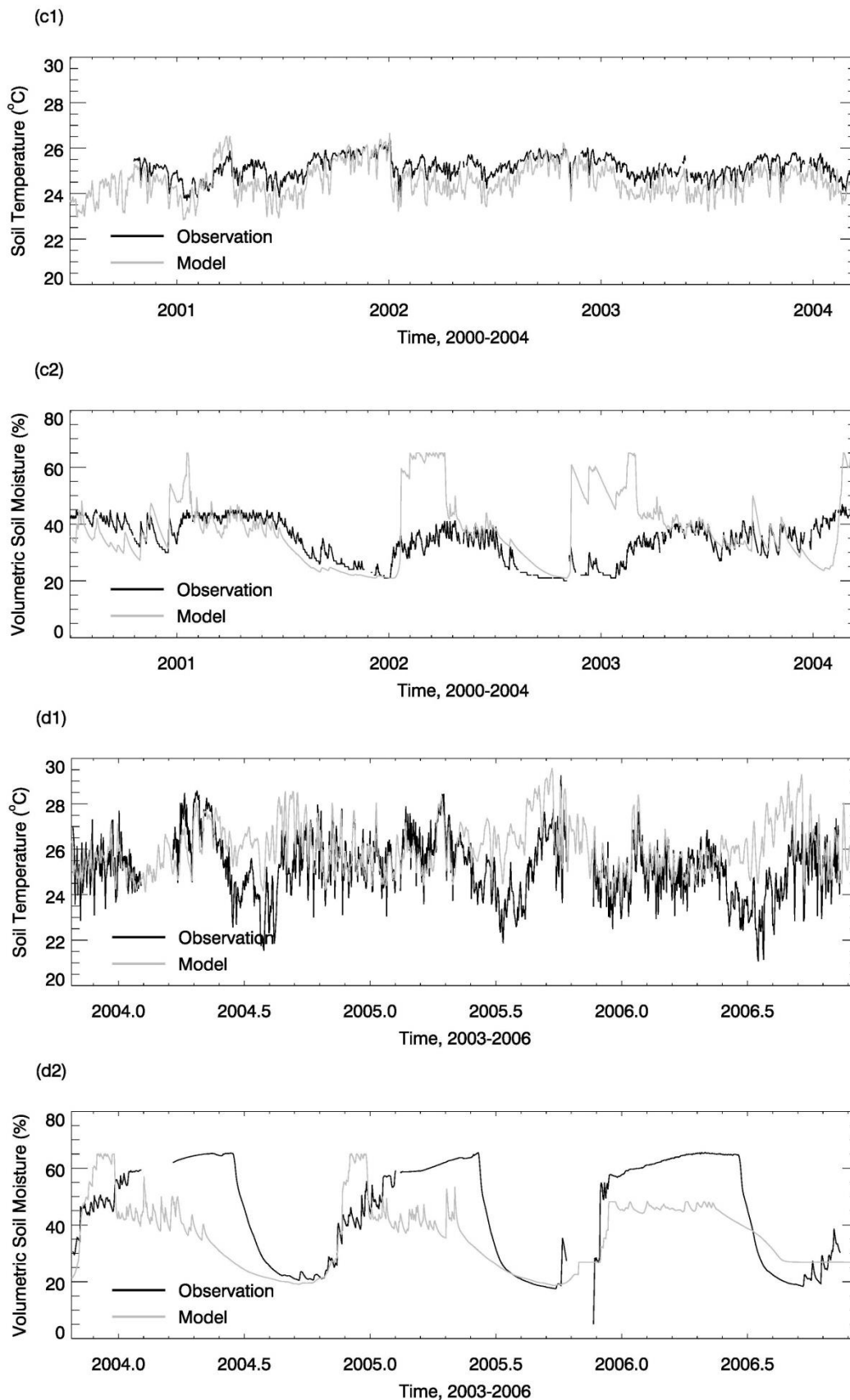
Figure 2. Contd. Evaluation of thermal and hydrology module at four sites: (c) Tropical Moist Forest, (d) Tropical Forest-Savanna. (1) shows the soil temperature comparison between the model simulations (gray line) and observations (black line) and (2) shows the soil moisture comparison between the model simulations (gray line) and observations (black line)
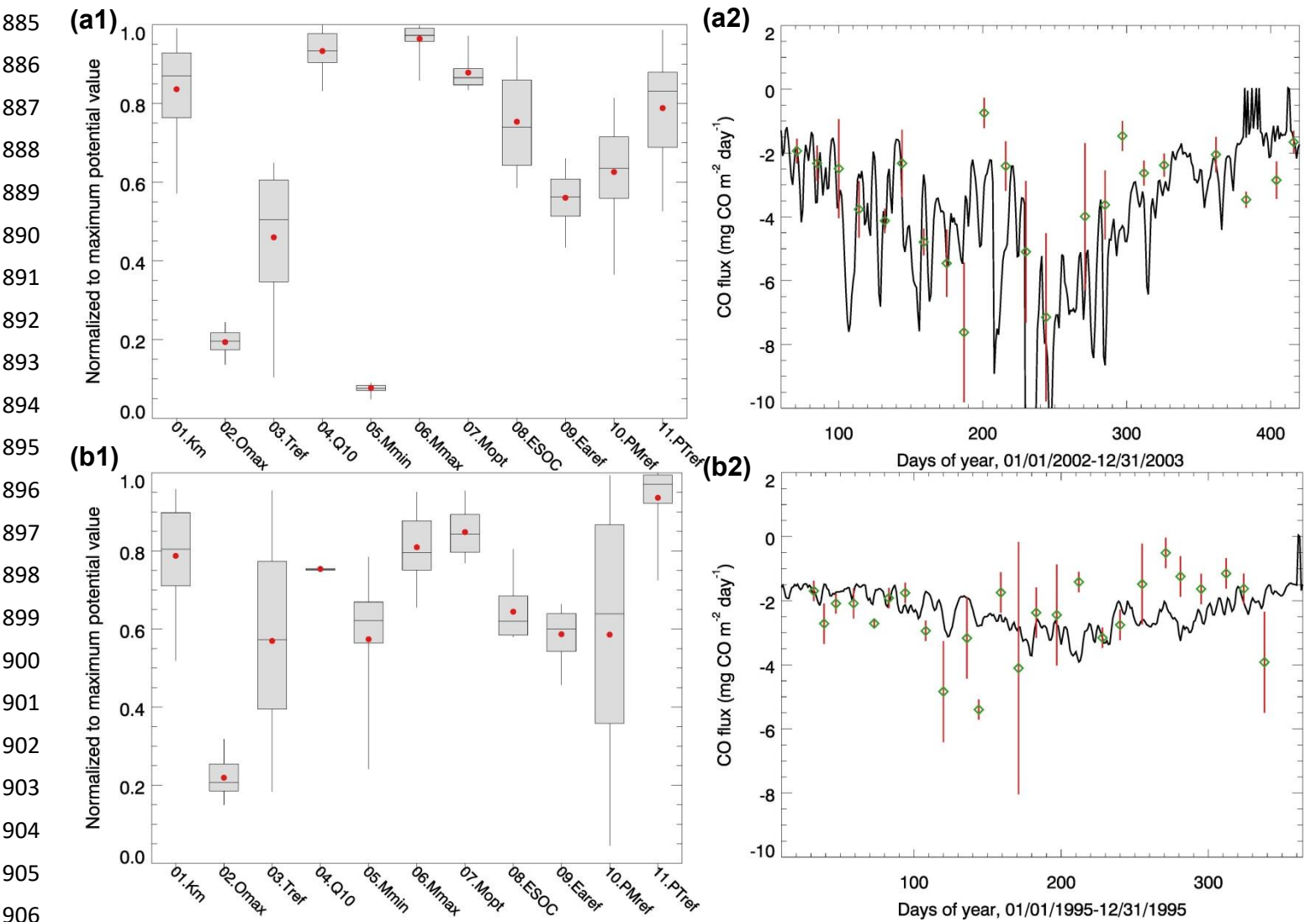
907 **Figure 3.** Parameter ensemble experiment results: Each parameter has 50 calibrated values generated from running SCE-

908 UA-R 50 times independently. Parameters are normalized to their largest potential values described in Table 2. (a1) and

909 (a2) are temperate coniferous forest normalized parameter distribution boxplots and CO flux comparisons between the

910 model simulations (solid line, using mean value of parameters) and observations (green diamond, red lines represent error

911 bar, site No.8), respectively. For each box, line top, box top, horizontal line inside box, box bottom and line bottom represent

912 maximum, third quartile, median, first quartile and minimum of 50 parameter values. Red dot represents the mean value of

913 50 parameter values. (b1) and (b2) are plots for temperate deciduous forest (site No.11).
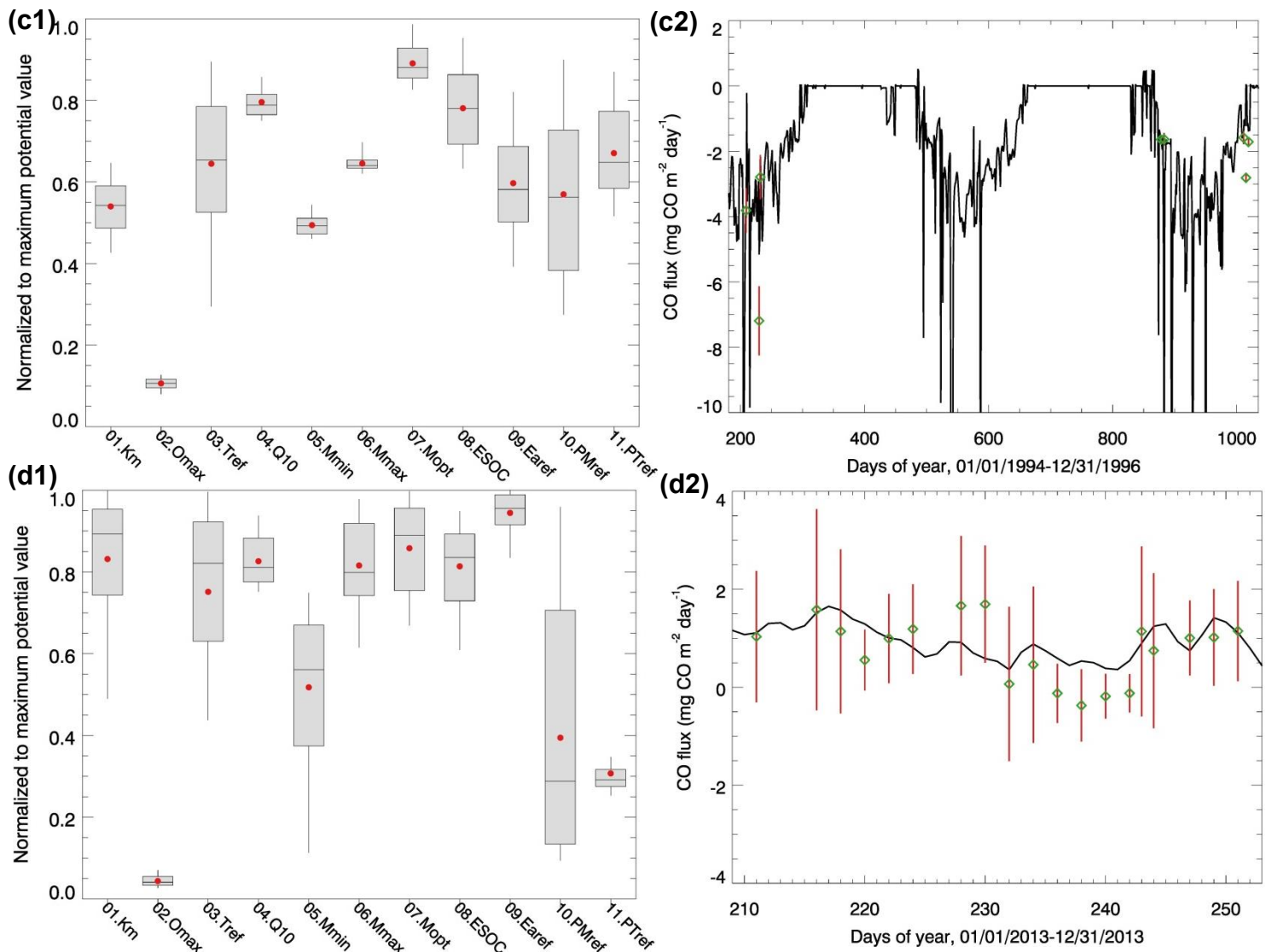
Figure 3. Contd. Parameter ensemble experiment results: Each parameter has 50 calibrated values generated from running SCE-UA-R 50 times independently. Parameters are normalized to their largest potential values described in Table 2. (c1) and (c2) are boreal forest normalized parameter distribution boxplots and CO flux comparisons between the model simulations (solid line, using mean value of parameters) and observations (green diamond, red lines represent error bar, site No. 12), respectively. For each box, line top, box top, horizontal line inside box, box bottom and line bottom represent maximum, third quartile, median, first quartile and minimum of 50 parameter values. Red dot represents the mean value of 50 parameter values. (d1) and (d2) are for grassland (site No.6). Grassland observation data is the sum of hourly observations so error bar represented the standard deviation.

941
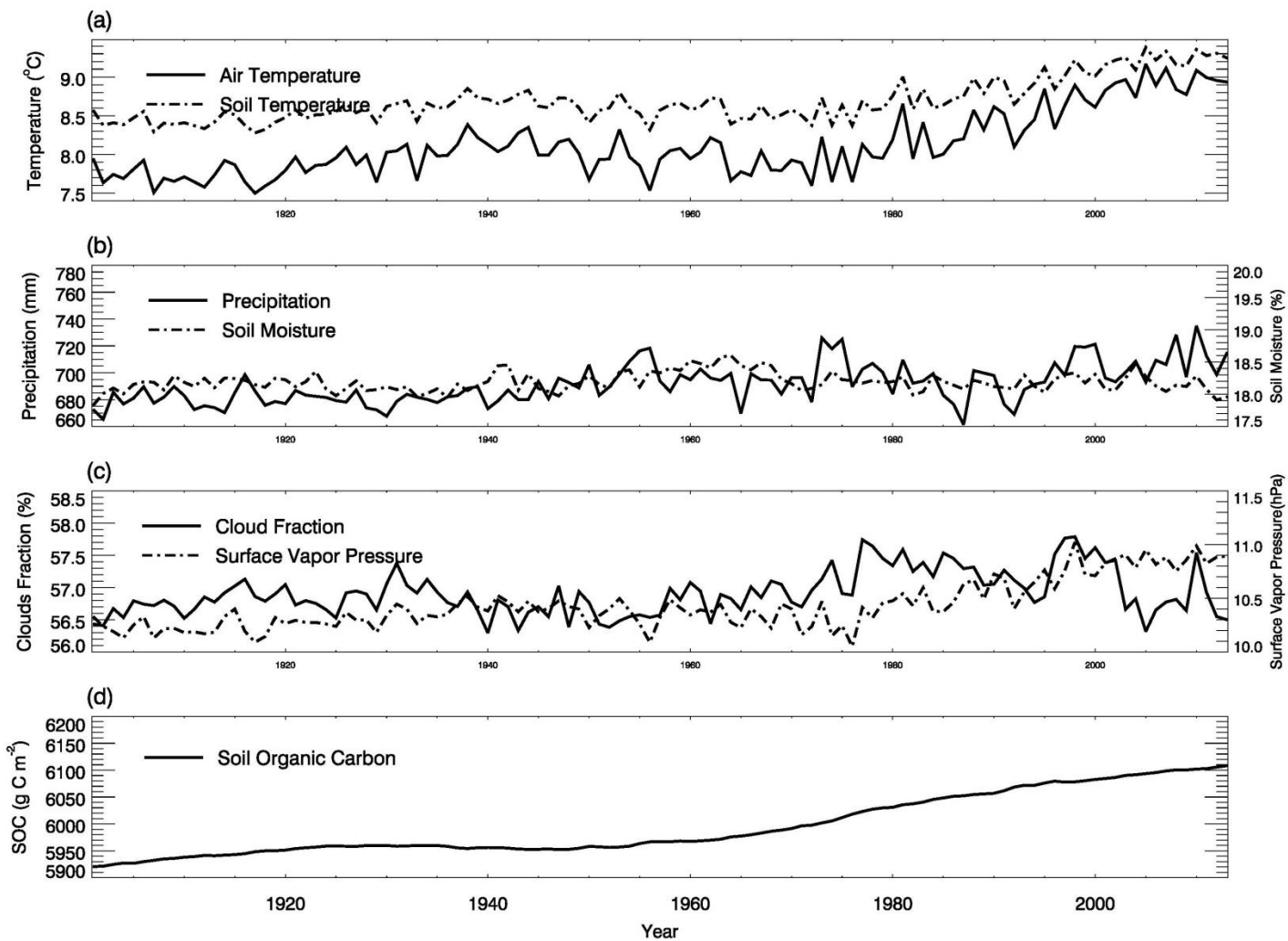
Figure 4. Historical global land surface (excluding Antarctic area and ocean area) mean climate, and simulated global mean soil moisture, soil temperature and SOC for the period 1901-2013.

944

945
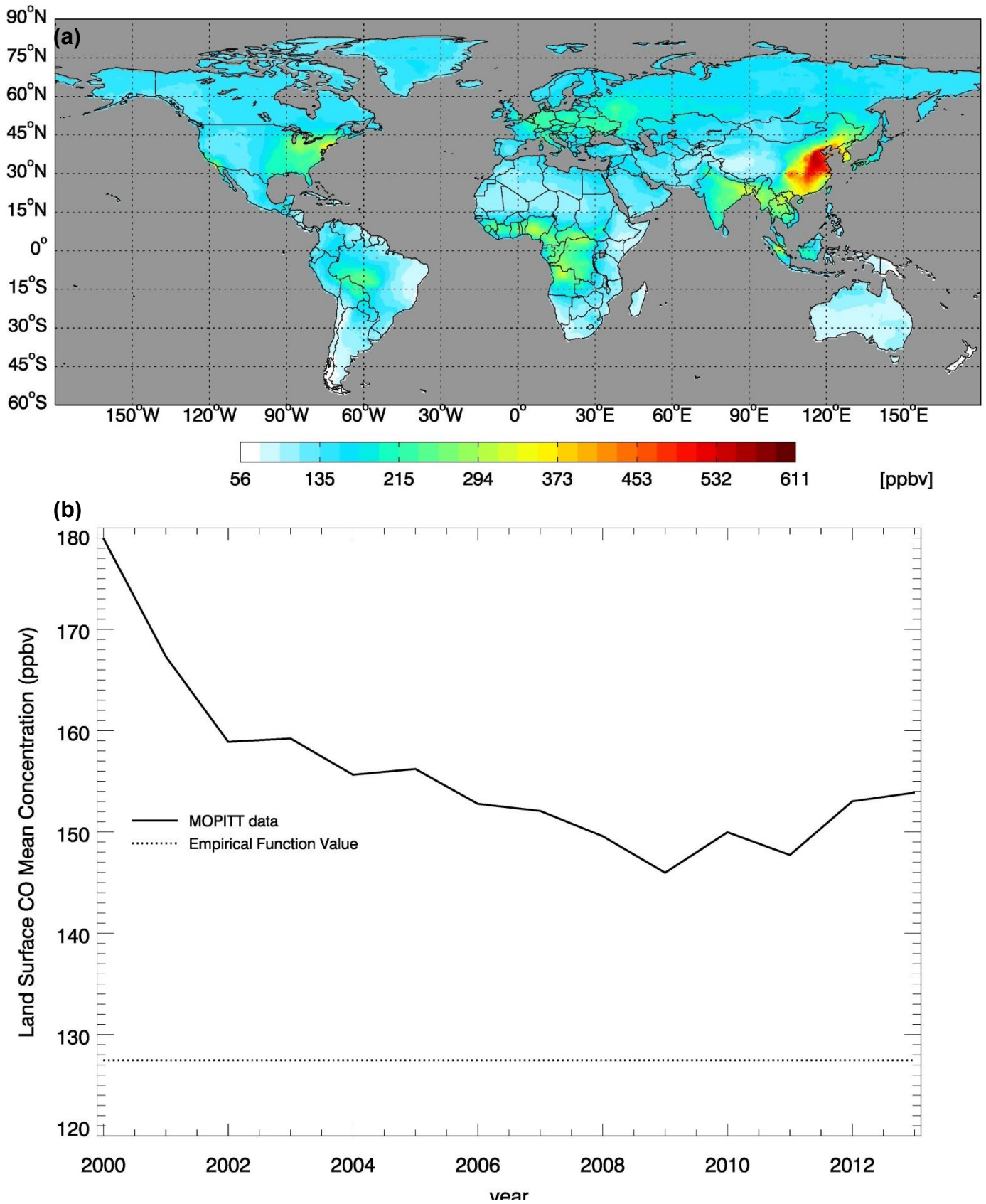
Figure 5. CO surface concentration data from MOPITT satellite (ppbv): (a) the global mean CO surface concentrations from MOPITT during 2000-2013; (b) the CO annual surface concentrations from both MOPITT and empirical functions (Potter et al., 1996).
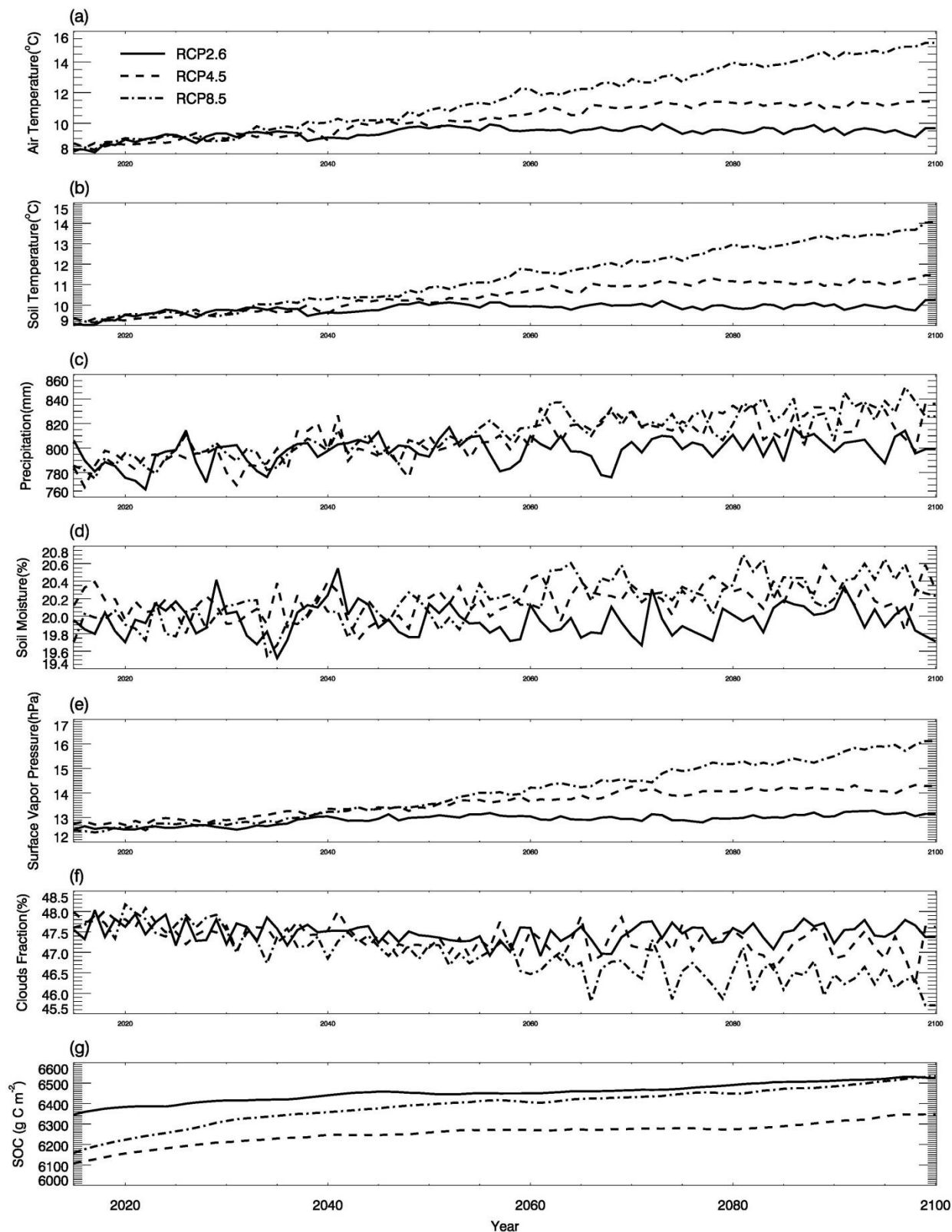
Figure 6. Global land surface (excluding Antarctic area and ocean area) mean climate from the RCP2.6, RCP4.5 and RCP8.5 data sets and simulated mean soil temperature, moisture and SOC: (a)-(g) are land surface air temperature (°C), soil temperature (°C), precipitation (mm), soil moisture (%), surface water vapor pressure (hpa), cloud fraction (%), and SOC (mg m^{-2}), respectively.
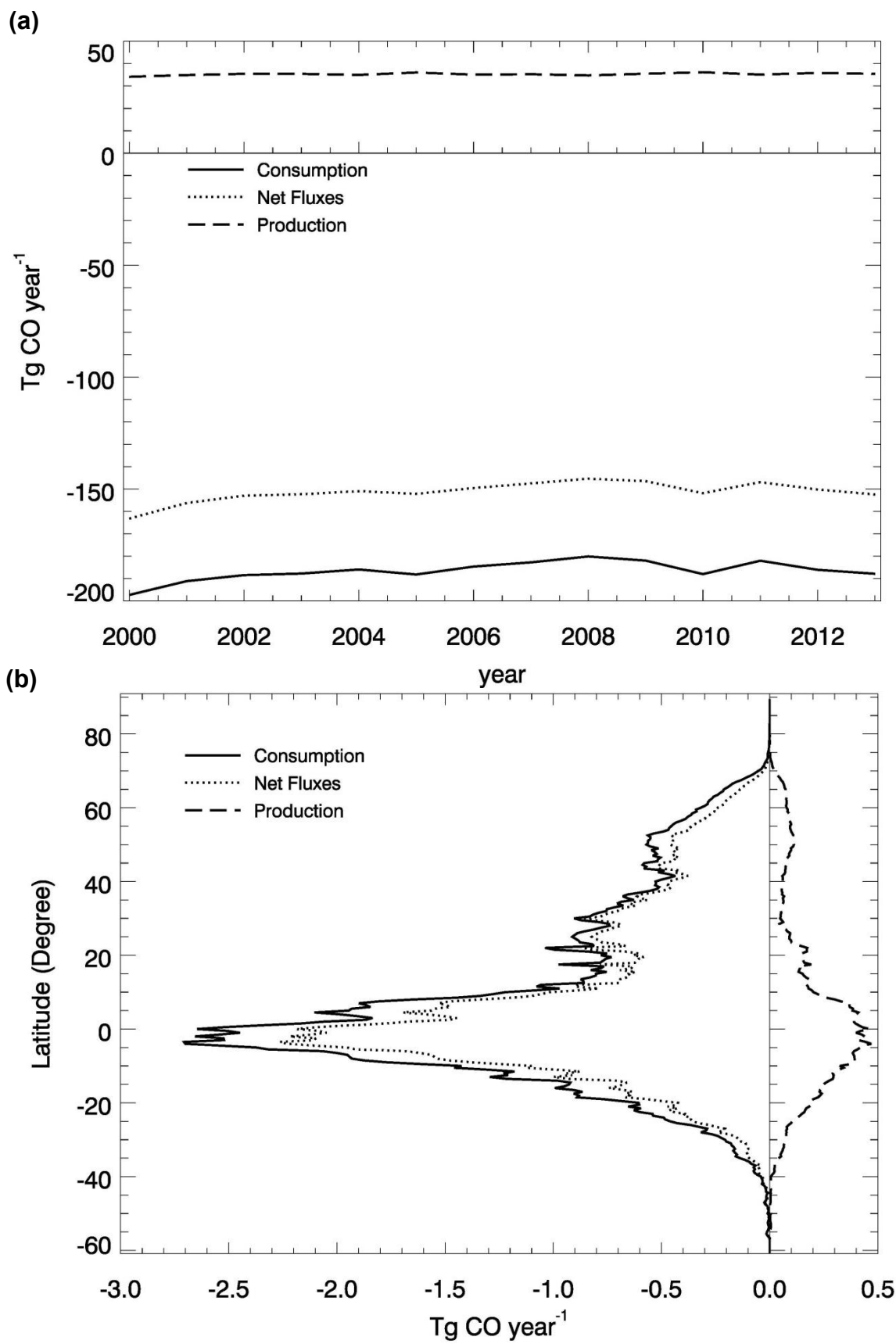
Figure 7. Global mean soil CO consumption, production and net flux: (a) the annual time series during 2000-2013and (b) the latitudinal distribution during 2000-2013.

032

033
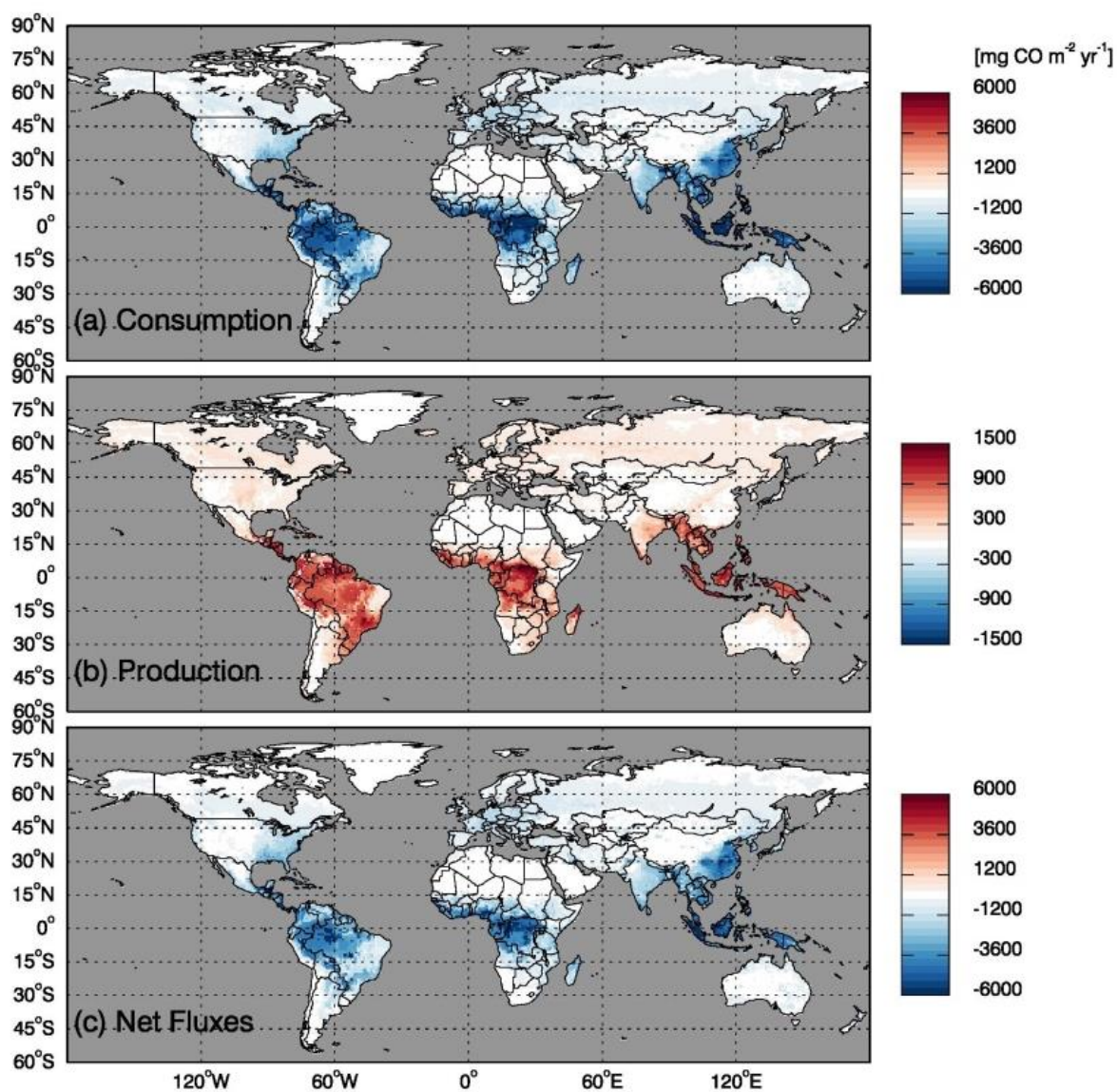
Figure 8. Global annual mean soil CO fluxes (mg CO m^{-2} yr^{-1}) during 2000-2013 using the MOPITT CO atmospheric surface concentration data

034
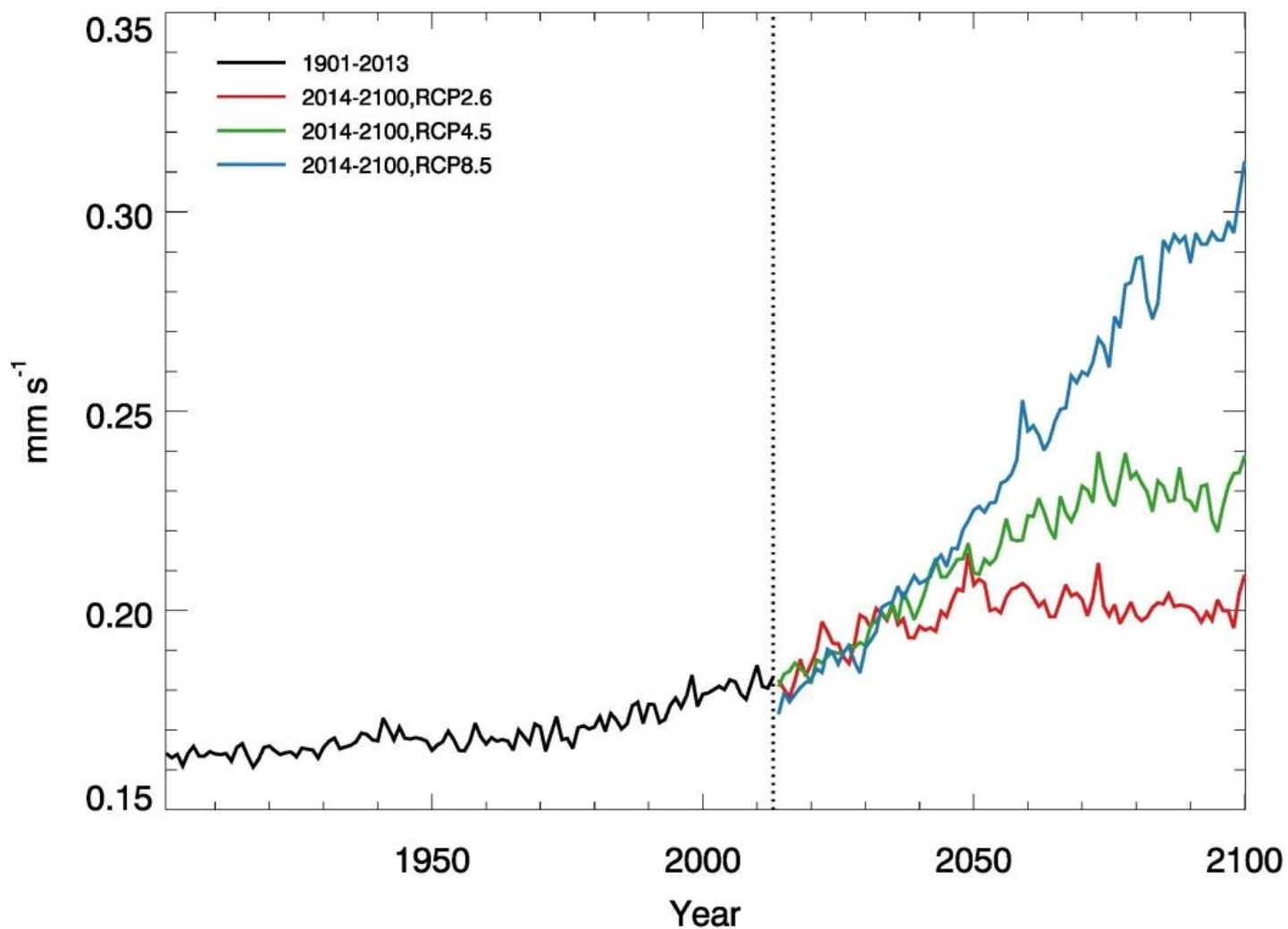
035 **Figure 9.** Global mean annual time series of CO deposition velocity (mm s^{-1}) using constant in time and spatially
036 distributed CO concentration data during 1901-2013 (left side of the dot line) and under the future climate scenarios
RCP2.6, RCP4.5 and RCP8.5 during 2014-2100 (right side of the dot line)

037

038
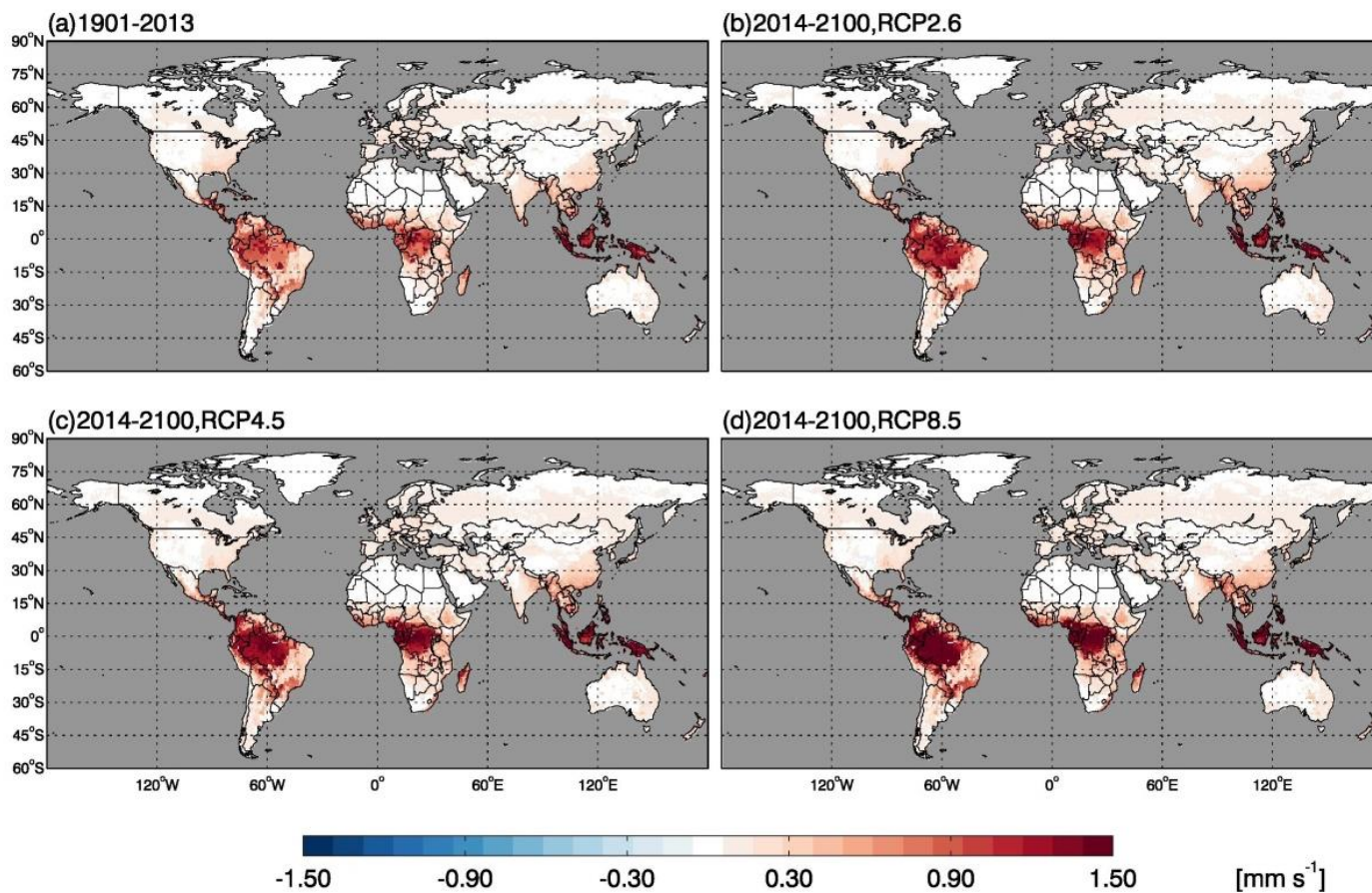
039 **Figure 10.** Global annual mean CO deposition velocity using constant in time and spatially distributed CO
concentration data (mm s^{-1}) a) during 1901-2013 and b), c), d) under the future climate scenarios RCP2.6, RCP4.5
040 and RCP8.5 during 2014-2100, respectively,

041
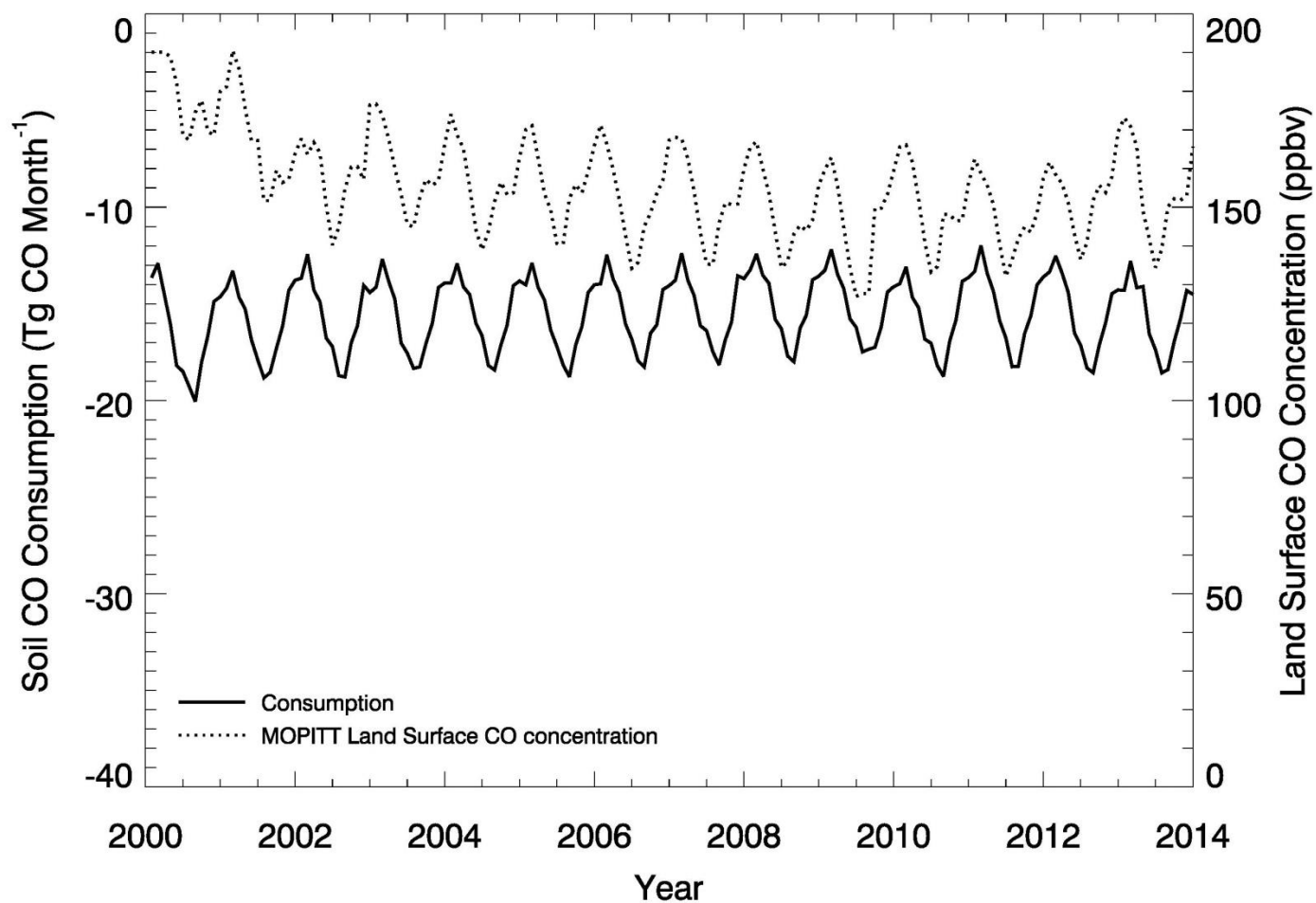
042 **Figure 11.** Global mean monthly time series of the MOPITT surface atmospheric CO concentration (ppbv) and soil CO consumption from model simulations E1 (Tg CO mon^{-1})
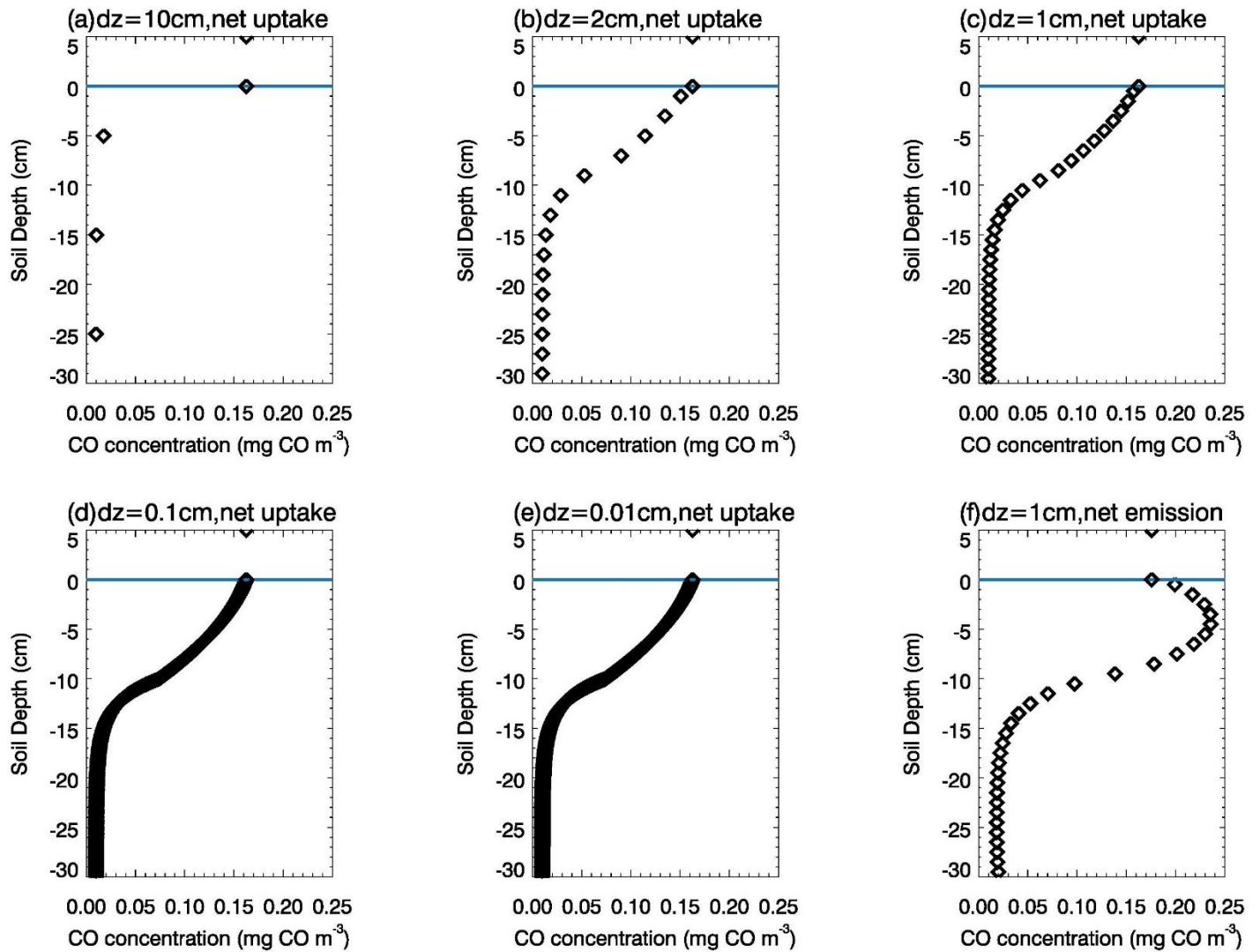
Figure 12. Daily mean vertical soil CO concentration profiles of top 30 cm. In the soil (depth < 0 cm), black diamonds represent the soil CO concentration (mg CO m^{-3}). Above the surface (depth>=0 cm), black diamonds represent the atmospheric CO concentration. a), b), c), d) and e) are the results from the same day when soils are a net sink of CO, but using different layer thickness (dz = 10 cm, 2 cm, 1 cm, 0.1 cm and 0.01 cm, respectively); f) is the result from the day when soils are a net source of CO, with dz = 1 cm.